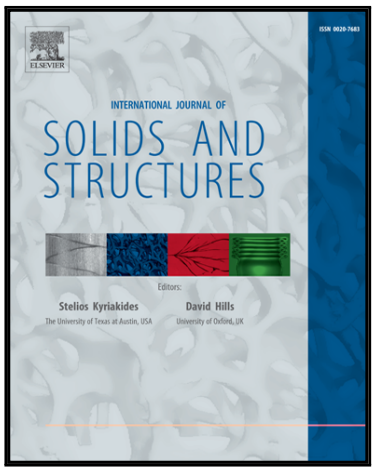

A parametric study of the mechanical and dispersion properties of cubic lattice structures

L. Junyi, D. Balint

PII: S0020-7683(16)30052-X
DOI: 10.1016/j.ijsolstr.2016.04.028
Reference: SAS 9149

To appear in: *International Journal of Solids and Structures*

Received date: 5 September 2015
Revised date: 5 February 2016
Accepted date: 19 April 2016

Please cite this article as: L. Junyi, D. Balint, A parametric study of the mechanical and dispersion properties of cubic lattice structures, *International Journal of Solids and Structures* (2016), doi: 10.1016/j.ijsolstr.2016.04.028

A parametric study of the mechanical and dispersion properties of cubic lattice structures

L. Junyi[a,*], D. Balint[a]

[a]*Imperial College London, Mechanical Engineering Department, South Kensington Campus, London SW7 2AZ.*

Abstract

A study of the mechanical and dispersion properties of cubic lattice structures have been conducted to assess the viability of designing a multifunctional and lightweight lattice structure with excellent static properties and elastic band gaps for vibration attenuation. In this study, the parameters that characterises the mechanical properties for stiffness and strength to be used as sandwich structure core materials were identified. A parametric study on the geometry of the lattice structures on the static properties was performed in order to determine the optimal geometry for these applications. The trends relating the geometric parameters to the mechanical properties of the lattice topologies were found and discussed. Local resonators were then added to the optimal geometries to create the band gaps that will attenuate vibrations at given frequency ranges. The tuned frequency was set to be 500 Hz in this study. The effects of the geometric parameters on the band gap widths produced by the introduction of the resonators were studied and the trends were found to be similar for all topologies. The results of this study indicate that the addition of local resonators to introduce band gaps is only viable when the stiffness and strength of the lattice without the resonators are sufficiently large, so that the increase in density will not be too significant. Lastly, band gaps around the tuned frequencies were observed for one of the topologies without the resonators. Since these band gaps do not result in an increase in mass, tuning the geometry to move the band gaps to the desired frequency ranges is a preferred strategy over the addition of local resonators.

Keywords: Multifunctional structures, band gap, Bloch wave theory, band structure, elastic metamaterials, periodic structures, lattice materials, cubic topologies, lightweight structures

1. Introduction

Lattice materials are cellular structures composed of periodically repeating unit cells. These materials can be engineered to have several unique properties, such as having high strength to density ratio [1, 2], high stiffness to density ratio [1, 2], low thermal coefficient with high stiffness [3–5], and elastic band gaps, which are regions of frequencies that prevent elastic waves from propagating [6–8]. Since lattice materials can be designed to have several desirable properties, they have huge potential to be used in multifunctional applications, including ultralight structures, impact absorbers, heat dissipation, vibration control, and many others.

The multi-functionality of lattice materials enables it overcome several issues that cannot be resolved with conventional bulk materials. Among these issues is the conflicting requirements of stiffness and vibration control of structural components. In order to sustain huge loads without large static displacements or compromising structural integrity, structural components generally require high stiffness [9, 10]. However, structures with high stiffness are also sensitive to vibrations, which may threaten the structural integrity of the system. A possible solution to minimise the trade-off between vibration attenuation and stiffness is

*Corresponding author
Email address: junyi.lee108@imperial.ac.uk (L. Junyi)

to exploit the high stiffness and strength to density ratios present in selected lattice structures [11, 12] and embedding local resonators, as seen in several studies [9, 13–15], to produce band gaps that will attenuate vibrations. With current three-dimensional printing technology, lattice structures with the embedded local resonators can be manufactured, allowing the potential of the multi-functionality of lattice structures to be realised.

Currently, there are a large number of studies that have been conducted on the analysis of the static mechanical (stiffness and strength) [1, 16–22] and dispersion properties of lattice materials [6–8, 15, 23, 24]. However, only a few studies [9, 13, 14, 25] have investigated these two types of properties in tandem or the design of a stiff structural material with desirable dynamic characteristics. Therefore, this paper aims to contribute to the design of elastic metamaterials with desirable dynamic properties, while having other qualities, like high stiffness, so that it can be implemented in practical situations. This is an important feature of elastic metamaterials as highlighted in [26]. The parametric study of the effects of the geometry on the static mechanical and dispersion properties will serve as a guide for future designs of multifunctional components and encourage future research in this type of materials.

In this study, the mechanical and dispersion properties of four cubic lattice topologies with internal resonators, similar to the designs seen in [15], were studied. Firstly, a parametric study on the lattice geometry, which are the lengths and radii of the lattice struts, was performed to determine the combination of geometric parameters that give the optimal mechanical properties. Local resonators consisting of struts with a point mass at one of its ends will then be attached to the lattices with the best mechanical properties to produce the local resonant band gaps. The width and location of the band gaps resulting from the addition of local resonators of different sizes and masses will be investigated. Lastly, the increase in density was also calculated to determine the penalty of adding the resonators and to assess if this strategy is viable.

2. Selected Topologies And Analysis Procedures

2.1. Selected topologies and resonators

Four cubic lattice topologies, which are the simple cubic, body centred cubic (BCC), face centre cubic (FCC), and octet truss structures, to be used as core materials in sandwich structures were studied. The unit cells of these topologies including the local resonators are shown in Fig. 1. Several of the beams in the unit cells were omitted to avoid overestimating the strength and stiffness through duplication. The lattice structures will consist of the *base* lattice structures and the added local resonators, which are beams with a point mass, for example a ball bearing, at the end. This facilitates the manufacturing of the local resonators as materials other than the strut materials can be used for the mass, which can be attahced easily via other strategies like adhesives.

There are several reasons for the selection of these topologies. Firstly, the addition of the resonators to these lattices are straightforward and since the resonators do not contribute to the strength or stiffness of the material, the mechanical properties and dispersion properties can be investigated independently. Additionally, cubic lattice structures can be easily manufactured using currently available three-dimensional printing technologies. The natural frequencies of the local resonators, and the location of the band gap, can also be easily tuned without making any changes to the base structure.

Although other methods to create LR band gaps, such as adding masses at the nodes [24] or manipulating the connectivity of the struts as discussed in [27] can be used to introduced band gaps, the key reason that the topologies in Fig. 1 were selected over the other architectures is because the natural frequencies of the resonators can be found easily. This facilitates the selection of the geometric parameters and mass of the resonators to achieve the required tuned frequencies. The calculations for the target frequencies by adding masses at the nodes are less straightforward than the cantilever resonators in the selected designs. Furthermore, the lattice structure studied here is intended to be used as a lightweight structural component, with high stiffness and low mass, suggesting that the struts are likely to be stiff. Since the natural frequency increases with increasing stiffness and reducing mass, the strategy of adding masses at the nodes may lead to large masses being required for a given target frequency. Conversely, the resonators that do not take any load can be designed to have low stiffness and a lower mass can be used to achieve the same natural

frequency. This provides more design flexibility. Similarly, the manipulation of the strut connectivity will result in significant changes in the static mechanical properties, which complicates the analysis significantly.

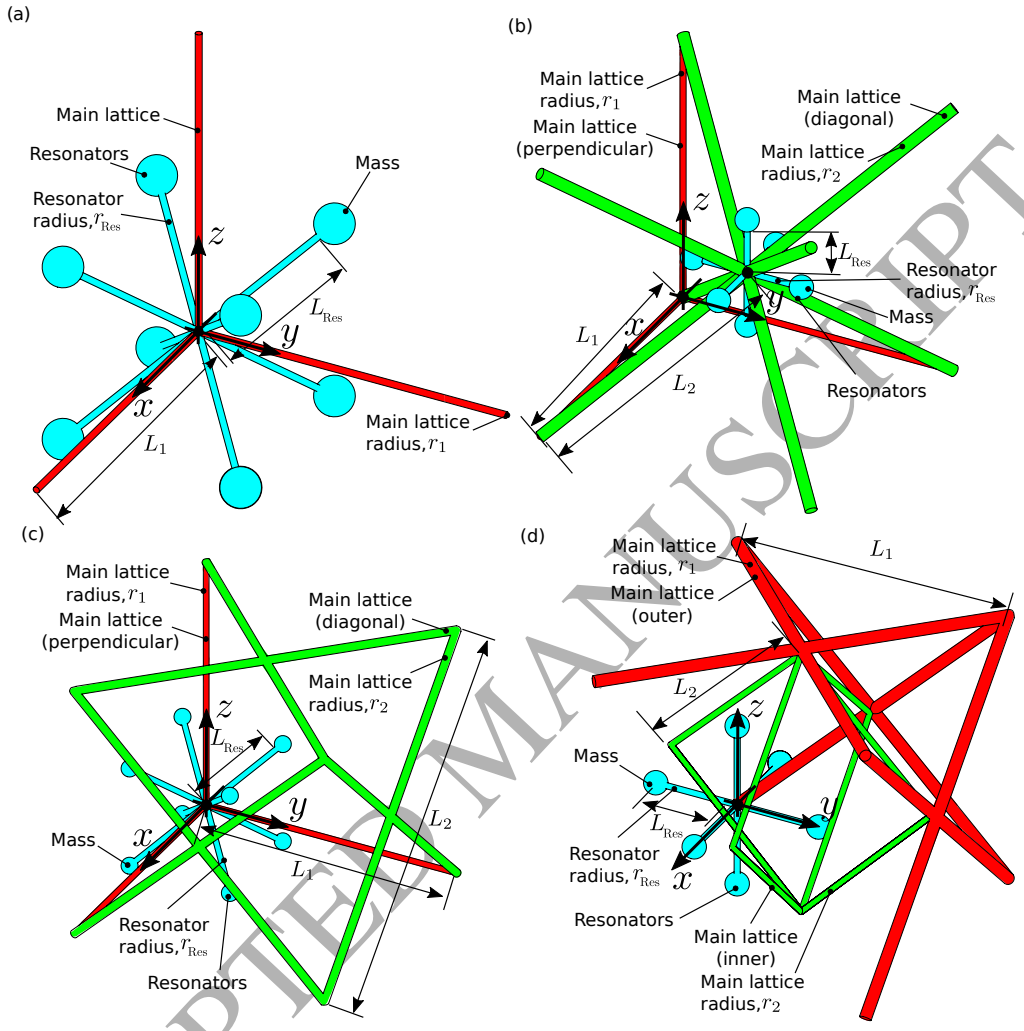

Figure 1: Selected topologies and the added resonators (a) Simple Cubic (b) BCC (c) FCC (d) Octet truss.

The ratios characterising the structural performance of core materials in lightweight sandwich panels and beams according to [12] are summarised in Table 1. The ratios in the table were obtained using the analysis from [28], which will be described briefly. For a beam or panel being loaded as shown in Fig. 2 to be used in lightweight applications, the mass of the beam or panel, m, defined in Eq. (1) must be minimised. For a beam the width, W, and height, H, are equal while a panel is assumed to have a fixed width, W,

$$m = \rho(WHL) \tag{1}$$

where ρ is the density of the material and W, H, and L are the dimensions shown in Fig. 2.

However, as a structural bearing component, the beam or panel must be able to either have a sufficient amount of stiffness (stiffness constrained) to minimise deflection or sufficient strength (strength constrained) to prevent failure. Therefore, the minimum stiffness, S_E and strength, S_σ are defined in Eq. (2) and Eq. (3) respectively. These equations are easily derived based on the Euler-Bernoulli beam theory and although

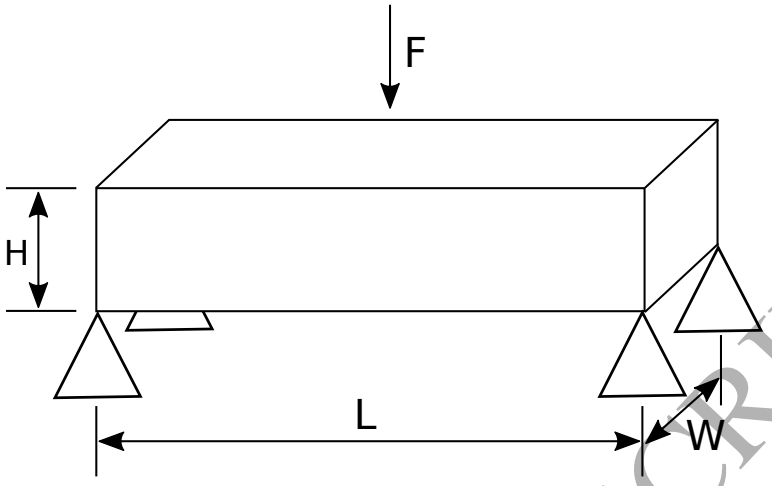

Figure 2: Beam and panel being loaded.

Fig. 2 shows a point load condition, the equations for other loading conditions can be found by varying the variable C. Interested readers can refer to [28] for the derivations of the equations and values of C.

$$S_E \leq \left(\frac{F}{\delta}\right) = \left(\frac{CWH^3}{12L^3}\right) E \tag{2}$$

$$S_\sigma \leq \left(\frac{F}{WH}\right) = \left(\frac{CWH^2}{6L}\right) \sigma_f \tag{3}$$

where S_E and S_σ are the stiffness and strength constraints, F is the force, δ is the deflection, E is the Young's modulus, and σ_f is the failure stress.

According to Eq. (1), the values of H and W for the beam, and H for the panel can be varied freely. The restrictions of the stiffness and strength constraints are imposed by substituting Equations (2) and (3) into Eq. (1) to eliminate $H = W$ for the beam, or H for the panel.

$$m = \left(\frac{12S_E L^3}{C}\right)^{\frac{1}{2}} L \left(\frac{\rho}{E^{\frac{1}{2}}}\right) \tag{4}$$

$$m = \left(\frac{6S_\sigma L}{C}\right)^{\frac{2}{3}} L \left(\frac{\rho}{\sigma_f^{\frac{2}{3}}}\right) \tag{5}$$

$$m = \left(\frac{12S_E L^3}{CW}\right)^{\frac{1}{3}} WL \left(\frac{\rho}{E^{\frac{1}{3}}}\right) \tag{6}$$

$$m = \left(\frac{6S_\sigma L}{CW}\right)^{\frac{1}{2}} WL \left(\frac{\rho}{\sigma_f^{\frac{1}{2}}}\right) \tag{7}$$

Therefore, the mass that needs to be minimised for the beam (stiffness constrained), beam (strength constrained), panel (stiffness constrained), and panel (strength constrained) can be expressed as Eq. (4), (5), (6), and (7) respectively. The important ratios to be minimised relating to material selection can be determined from these equations, and their inverses that are to be maximised are listed in Table 1. These ratios will be referred to as the strength and stiffness parameters.

Configuration	Strength Constrained	Stiffness Constrained
Beam	$\frac{\sigma_f^{\frac{2}{3}}}{\rho}$	$\frac{E^{\frac{1}{2}}}{\rho}$
Plate	$\frac{\sigma_f^{\frac{1}{2}}}{\rho}$	$\frac{E^{\frac{1}{3}}}{\rho}$

where σ_f is the failure stress, E is the Young's modulus, and ρ is the density.

Table 1: Ratios to maximise for beam and plate configurations [12].

In this paper, a parametric study was performed by setting the length of the unit cell, L_1, to 50 mm and studying the stiffness parameter, strength parameter, and band gap width with varying geometries. The range of the normalised geometry parameters studied are summarised in Table 2. Additionally, the material selected to construct the lattice structures was acrylonitrile butadiene styrene (ABS) and its mechanical properties are listed in Table 3. The selected dimension ranges and material can be typically produced using common three dimensional printing technologies, so that the results of this study can serve as a reference for future studies with 3D printed parts. An important point to note is that 3D printing has been known to introduce anisotropy and reduce the stiffness and strength of the materials [29, 30]. Anisotropy in 3D printed materials is a result of the material being deposited directionally and this is likely to affect the predicted lattice behaviour, where the material was assumed to be isotropic in this study. Since this study mainly focuses on the trends and properties of the lattice structures, the effects of the anisotropy will not be studied. Additionally, other improvements have been made in 3D printing technology to reduce the effects of anisotropy, for example in [29], while other lattice production techniques, such as weaving [31] may result in better material behaviour. Hence, the results in this study can serve as a reference for an initial design and further work should be done to account for the anisotropy of 3D printed parts.

Ratios	Minimum value	Maximum value
$\frac{r_1}{L_1}$	0.01	0.20
$\frac{r_2}{r_1}$	0.50	1.50
$\frac{L_{\text{Res}}}{L_1}$	0.05	0.25
$\frac{r_{\text{Res}}}{r_1}$	0.30	1.50

Table 2: Dimensions that were investigated in this study.

Property	Value	Units
Young's modulus, E	3.29	GPa
Shear modulus, G	1.18	GPa
Density, ρ	1200	kg m^3
Yield strength, σ_y	53	MPa

Table 3: Mechanical properties of ABS [32].

In addition to the static mechanical properties of the lattice, resonators that are tuned to the target frequency will be introduced into the main lattice, as seen in Fig. 1. The resonators are similar to dynamic absorbers and are used to introduce local resonant band gaps seen in [33, 34]. In this study, the resonance frequency was set to be 500 Hz for a cantilever configuration, that is within the same order of magnitude for the forcing frequency of typical machinery. The local resonators used in this study have a number of combinations of radius, length, and mass that can be tuned to a given target frequency. Therefore, in order to study the effects of these different combinations on the band gaps, the band structure of a range of normalised radius and length were studied, while the mass was varied based on the radius and length to give the target natural frequency. In this study, the local resonators were modelled using finite elements with a total of 20 beam elements and a point mass at the end, while the end without the mass was set to have

a displacement of zero. An eigenvalue analysis was performed on the stiffness and mass matrix for every value of radius, length, and mass of the resonator to determine the natural frequency of the first mode. The required mass to give a natural frequency of 500 Hz was then found by varying the value of the mass in an iterative process.

2.2. Analysis of mechanical properties

As described previously, the addition of the resonators does not affect the structural performance of the lattices and hence they were omitted in the analysis of the static properties. When a large number of unit cells are present in the system, homogenisation techniques can be used to find the effective properties of the lattice structures. There are several homogenisation methods for lattice and cellular materials that have been published, for example [1, 18, 21, 35]. In this paper, the method introduced in [18] was selected mainly because this method can be used with the finite element method, which is convenient as the band gap analysis also makes use of the finite element method. Additionally, the method in [18] is capable of calculating all components of the homogenised stiffness matrix, $\mathbf{K}$, as described by Eq. (8), the yield surface and buckling surface under different loading conditions. The method in [18] uses a multiscale approach to determine the macroscopic mechanical properties. Firstly, the macroscale displacements and deformation were applied to the lattice, in which the boundary nodes are assumed to have periodic displacements. The microscale stresses are then obtained from the displacements and the microscale deformation is then calculated by using a finite element model of the unit cell. The macroscale stresses were then calculated by treating it as the gradient of the strain energy density with respect to the macroscopic strains, which allows the stiffness matrix to be determined. Lastly, the macroscopic forces can be found by applying the virtual work principle. For the sake of brevity, the homogenisation method will not be described here and interested readers should refer to [18]. The homogenised stiffness matrix, $\mathbf{K}$, in Eq. (8) is the Voigt notation of the stiffness tensor, where α, β, and γ correspond to $\mathbf{C}_{1111}$, $\mathbf{C}_{1122}$, and $\mathbf{C}_{2323}$ respectively, in which $\mathbf{C}$ is the full stiffness tensor. The stiffness matrix in Eq. (8) suggests that the material has several symmetries.

$$\mathbf{K} = \begin{bmatrix} \alpha & \beta & \beta & 0 & 0 & 0 \\ \beta & \alpha & \beta & 0 & 0 & 0 \\ \beta & \beta & \alpha & 0 & 0 & 0 \\ 0 & 0 & 0 & \gamma & 0 & 0 \\ 0 & 0 & 0 & 0 & \gamma & 0 \\ 0 & 0 & 0 & 0 & 0 & \gamma \end{bmatrix} \tag{8}$$

The stiffness component, α, in Eq. (8) was used to find the stiffness parameters listed in Table 1 by treating it as equivalent to the Young's modulus, E. This is mainly because the Euler-Bernoulli beam theory was used to derived the required parameters that characterise lattice structure in Table 1, and α corresponds to the stiffness in the axial direction, which was assumed to be the loading conditions at the top and bottom of the beam under plane strain. The failure stresses were determined by assuming that an axial stress is acting on the material. The failure stress for yielding is taken to be the stress at the macroscopic scale when the stress at any point in the struts of the member is equal to the yield stress of the bulk material. For buckling, the corresponding stress stiffness matrix to the uniaxial loading condition, with a unit value of stress was first determined, and an eigenvalue problem based on the homogenisation method [18] was solved to find the smallest eigenvalue. Since the material will buckle when any of the eigenvalues reaches unity, the smallest value of the inverse of all the eigenvalues was taken as the failure stress. The detailed procedure for determining the buckling stresses are explained in [18].

2.3. Dispersion analysis

Once the optimal geometries for the parameters listed in Table 1 were found, local resonators were then introduced to these lattices to produce the desired elastic band gaps. A dispersion analysis was then performed in order to determine the location and width of the band gaps. The dispersion curves in the periodic lattices were determined by applying Bloch wave boundary conditions on the appropriate boundary nodes and calculating the eigenvalues. This technique is commonly used in many studies, such as [7, 36–38].

Since the finite element method was used, the equations of motion can be written as Eq. (9). The required stiffness matrix, $\mathbf{K}$, and mass matrix, $\mathbf{M}$, in Eq. (9) were found using the finite element method, in which the lattice struts were modelled using Timoshenko beams [39] and the mass being modelled as a point mass.

$$\left(\mathbf{K} - \omega^2 \mathbf{M}\right) \mathbf{u} = \mathbf{F} \tag{9}$$

where $\mathbf{u}$ and $\mathbf{F}$ are the displacements and external forces of the nodes.

The Bloch wave boundary conditions, described by Eqs. (10) and (11), at the required nodes were then applied to the displacements and forces at the boundary nodes. Since the reference node in the unit cells, shown in Fig. 1, is at the origin, $\mathbf{x}$ in Eqs. (10) and (11) was set to $[0, 0, 0]^T$.

$$\mathbf{u_{x+L}} = \left(e^{i\mathbf{k}\cdot\mathbf{L}}\right)\ \mathbf{u_x} \tag{10}$$

$$\mathbf{F_{x+L}} = \left(e^{i\mathbf{k}\cdot\mathbf{L}}\right)\ \mathbf{F_x} \tag{11}$$

where $\mathbf{x}$ is the coordinate of the nodes, $\mathbf{L}$ is the lattice constant which is equal to the lengths of the lattice structure L_1 at the directions corresponding to the boundary nodes, and $\mathbf{k}$ is the wave vector.

A matrix $\mathbf{T}$ was then used to express the displacements and forces in terms of the independent nodes as seen in Eqs. (12) and (13).

$$\mathbf{u} = \mathbf{T}\ \tilde{\mathbf{u}} \tag{12}$$

$$\mathbf{F} = \mathbf{T}\ \tilde{\mathbf{F}} \tag{13}$$

where $\tilde{\mathbf{u}}$ and $\tilde{\mathbf{F}}$ are the displacement and force vectors for the independent nodes.

This allows the Eq. (9) to be simplified to Eq. (14) that will result in the eigenvalue problem described by Eq. (15).

$$\left(\mathbf{T}^H\mathbf{K}\mathbf{T} - \omega^2\mathbf{T}^H\mathbf{M}\mathbf{T}\right)\tilde{\mathbf{u}} = \mathbf{T}^H\mathbf{T}\tilde{\mathbf{F}} \tag{14}$$

where the superscript H denotes the Hermitian transpose.

$$\left(\tilde{\mathbf{K}} - \omega^2\tilde{\mathbf{M}}\right)\tilde{\mathbf{u}} = 0 \tag{15}$$

The band structure was then found by solving the eigenvalue problem in Eq. (15) for different values of wave vectors, $\mathbf{k}$. Due to symmetry, only the wave vectors, $\mathbf{k}$, within the First Brillouin Zone need to be considered [40] in order to determine the location of the band gaps. The First Brillouin Zones for the lattice structures considered in this study are shown in Fig. 3. The results and discussions of the dispersion analysis will be presented in Section 4.

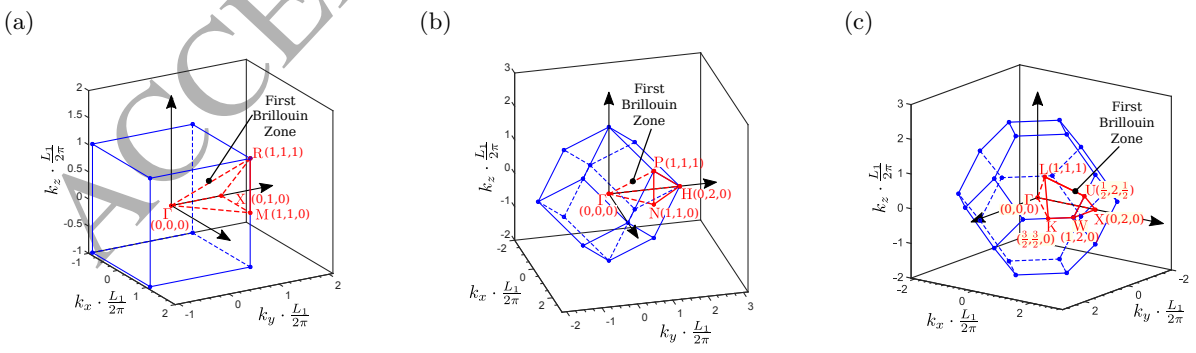

Figure 3: First Brillouin Zone of (a) Simple Cubic Lattice (b) BCC Lattice (c) FCC and Octet Lattice

3. Stiffness and strength properties of lattice materials

The stiffness and strength properties that characterises the performance of the lattice structures as core materials for sandwich panels or beams for the four topologies will be presented in this section. This is in order to determine the optimal geometry for the lattice prior to the introduction of the local resonators that generates the band gaps.

3.1. Simple cubic lattice

The stiffness and strength parameters for the lattice structures that have been calculated were normalised with respect to that for the bulk material. Therefore, a normalised parameter with a value greater than one indicates that the lattice structure is superior to the bulk material. These parameters for the simple cubic lattice in the panel and beam configurations are shown in Fig. 4 and Fig. 5 respectively. The normalised parameters were found to be independent of the length of the unit cells, L_1. Therefore, the only geometric parameter that can affect the static properties for the simple cubic structure is the radius to length ratio, $\frac{r_1}{L_1}$.

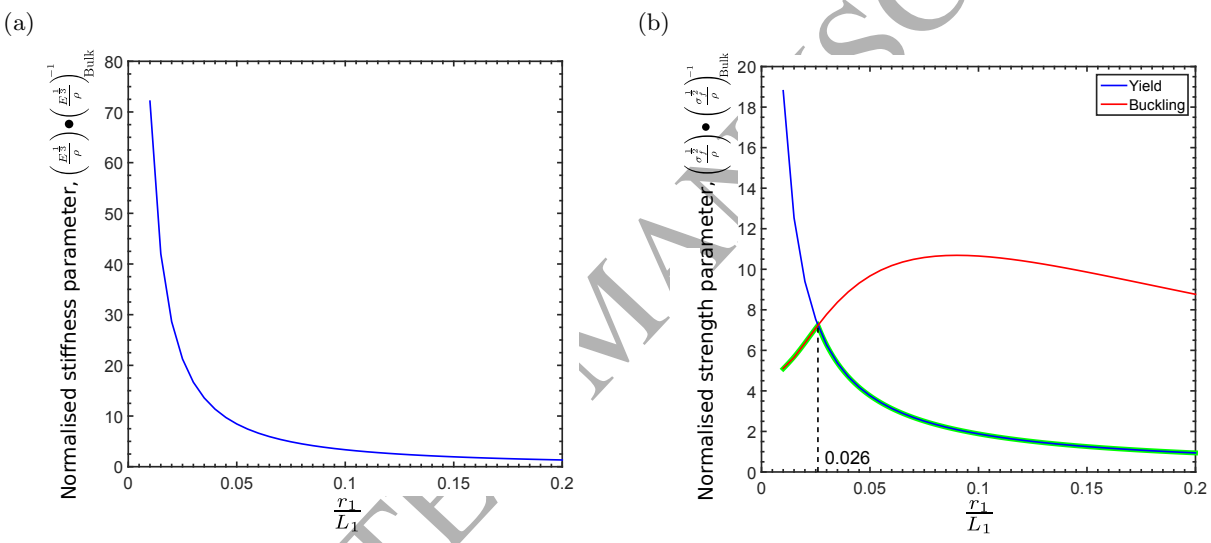

Figure 4: Static properties of the simple cubic structure with different radii for panel configurations (a) Normalised stiffness parameter (b) Normalised strength parameter.

As seen in Fig. 4 (a) and Fig. 5 (a), the normalised stiffness parameter reduces exponentially with increasing values of $\frac{r_1}{L_1}$. This result suggests that smaller radii are preferred for the simple cubic lattice in beam and panel configurations. Therefore, the lowest value of $\frac{r_1}{L_1}$ should be selected for the simple cubic lattice and minimum radii will be limited by either the strength of the lattice or manufacturing capabilities.

On the other hand, the normalised strength parameter for the two failure mechanisms, which are plastic yielding and buckling, for the panel and beam configurations are shown in Fig. 4 (b) and Fig. 5 (b) respectively. As seen in these figures, the normalised strength parameter for yielding, reduces exponentially with increasing $\frac{r_1}{L_1}$, like the normalised stiffness parameters. Conversely, the normalised strength parameter for buckling increases initially with increasing $\frac{r_1}{L_1}$ for both the panel and beam configuration. For the panel configuration, the normalised strength parameter for buckling will increase to a maximum value before decreasing again while for the beam configuration, the normalised strength parameter for buckling will continue to increase asymptotically. This trend is expected as the propensity for buckling decreases with decreasing slenderness.

Since the strength constrained simple cubic lattice panel and beam will fail once the stress reaches either the value for either yielding or buckling, the optimal value of $\frac{r_1}{L_1}$ is when the normalised strength parameter

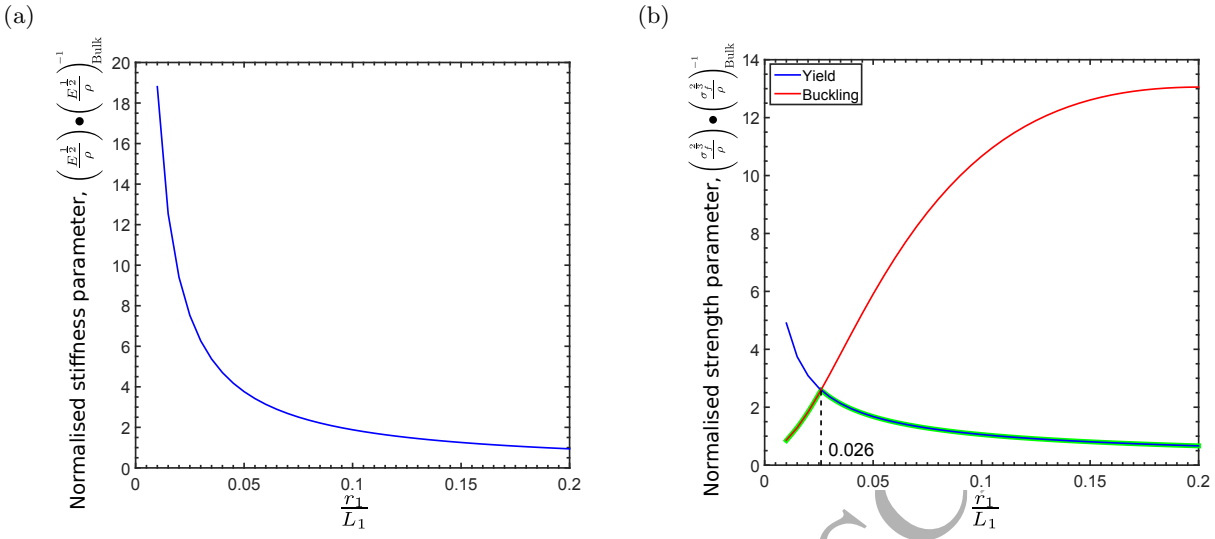

Figure 5: Static properties of the simple cubic structure with different radii for beam configurations (a) Normalised stiffness parameter (b) Normalised strength parameter.

for both failure modes are equal. The optimal value is shown in Fig. 4 (b) and Fig. 5 (b), and the normalised values of $\frac{r_1}{L_1}$ for both configurations are 0.026. The relatively low value of $\frac{r_1}{L_1} = 0.026$ will also produce relatively stiff simple cubic lattice panels and beams as the normalised stiffness parameter, seen in Fig. 4 (a) and Fig. 5 (a), are relatively high at this value.

3.2. Body-centred cubic (BCC) lattice

The normalised stiffness and strength parameters for the BCC lattice in the panel and beam configurations are shown in Fig. 6 and Fig. 7 respectively. Similar to the simple cubic lattice, the static properties for the BCC lattice were also found to be independent of the length of the unit cells, L_1. However, as seen in Fig. 1 (b), there are two sets of beams with different radii that were considered for the BCC structure. Thus, the two geometric parameters that will be analysed are $\frac{r_1}{L_1}$ and $\frac{r_2}{r_1}$.

As seen in Fig. 6 (a) and Fig. 7 (a), the normalised stiffness parameter reduces exponentially with increasing values of $\frac{r_1}{L_1}$, while increasing the values of $\frac{r_2}{r_1}$ will only increase this parameter slightly. Therefore, the optimal configuration of the BCC structure is to minimise $\frac{r_1}{L_1}$ and maximise $\frac{r_2}{r_1}$, but increasing $\frac{r_1}{L_1}$ will have a larger overall effect.

The normalised strength parameters for both the beam and panel configuration are shown in Fig. 6 (b) and Fig. 7 (b) respectively. The normalised strength parameters for yielding in both cases were found to decrease exponentially with increasing $\frac{r_1}{L_1}$, but they increase slightly with increasing $\frac{r_2}{r_1}$. Additionally, the normalised strength parameter for buckling, increases with both $\frac{r_1}{L_1}$ and $\frac{r_2}{r_1}$. This result is also expected as the propensity for the lattice to buckle decreases when the slenderness of the struts decreases.

The optimal configuration for the strength constrained panels and beams for the BCC lattice material is the region where the buckling and yielding parameters intersect, as highlighted by the red line in Fig. 6 (b) and Fig. 7 (b). As seen in Fig. 6 (b) and Fig. 7 (b), the optimal strength parameters appear to be insensitive to the values of $\frac{r_1}{L_1}$, in which the red line is always in between 0.0260 and 0.0398 for both the panel and beam configurations. However, as seen in both Fig. 6 (b) and Fig. 7 (b), the normalised strength parameter appears to increase with $\frac{r_2}{r_1}$ until a value and becomes constant after that. In order to investigate this further, the normalised strength parameter versus $\frac{r_2}{r_1}$ curves at the optimal $\frac{r_1}{L_1}$ values (the red line in Fig. 6 (b) and Fig. 7 (b)) are plotted in Fig. 8. As seen in Fig. 8, the normalised strength parameter will increase with $\frac{r_2}{r_1}$ until a local optimal value of 0.744 and 0.740 for the panel and beam configuration respectively. This result suggests that the inner beams seen in Fig. 1 for the BCC are the main cause of buckling failure

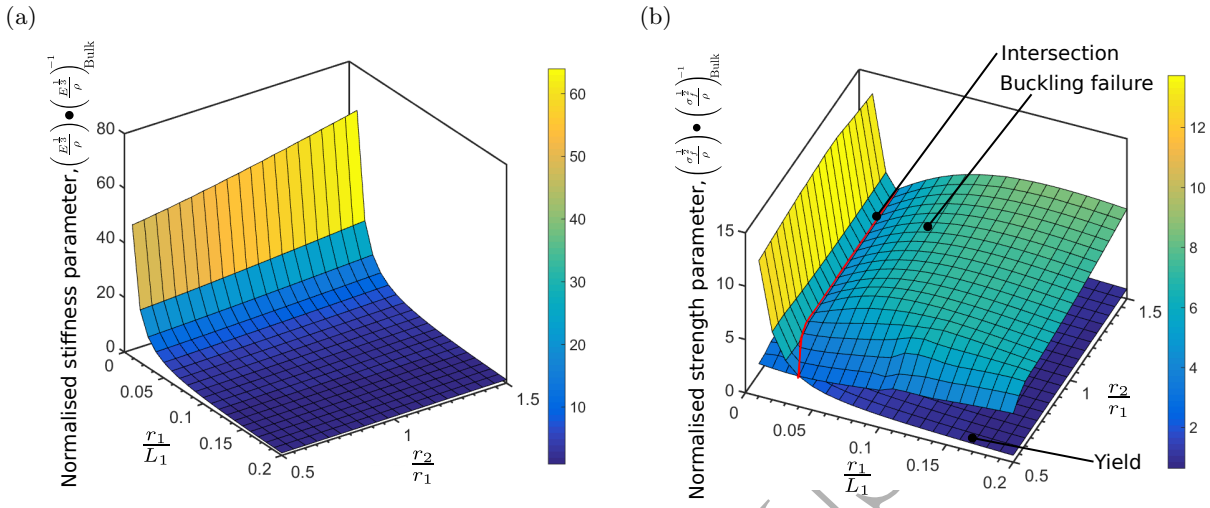

Figure 6: Static properties of the BCC lattice structure with different radii for panel configurations (a) Normalised stiffness parameter (b) Normalised strength parameter.

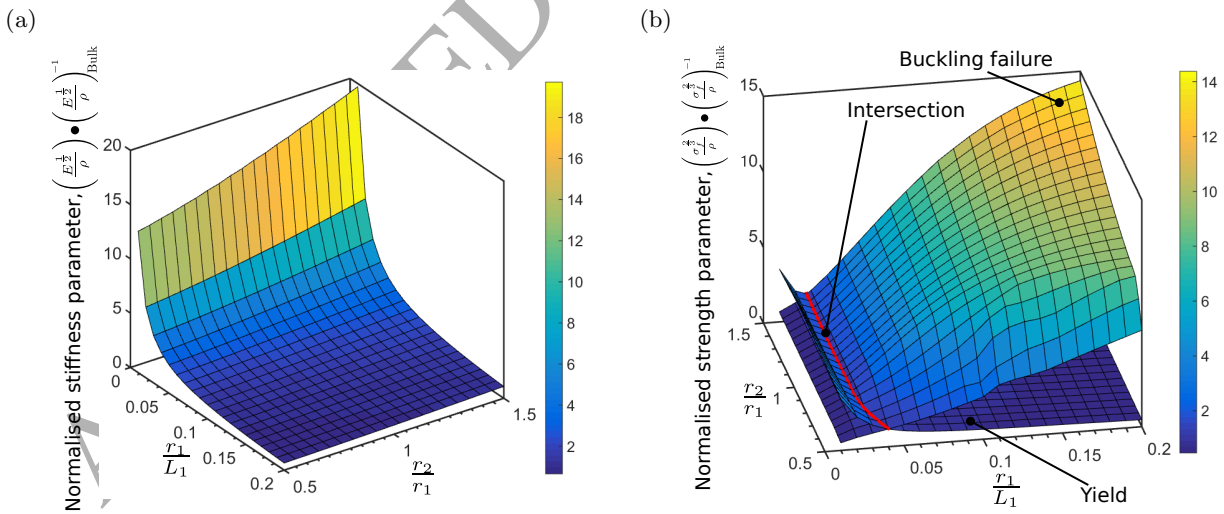

Figure 7: Static properties of the BCC lattice structure with different radii for beam configurations (a) Normalised stiffness parameter (b) Normalised strength parameter.

at $\frac{r_2}{r_1}$ values that are lower than the peaks shown in Fig. 8. Hence, the value of $\frac{r_2}{r_1}$ should be maximised for the BCC lattice. However, since the increase in strength after the peak values are relatively small and increasing the values of $\frac{r_2}{r_1}$ may require more material, the optimal configuration for the BCC lattice in this study is set to be at the peak in Fig. 8, which are $\frac{r_1}{L_1} = 0.027$, $\frac{r_2}{r_1} = 0.740$, (giving the normalised strength parameter of 4.374) for the panel and $\frac{r_1}{L_1} = 0.027$, $\frac{r_2}{r_1} = 0.744$, (giving the normalised strength parameter of 1.618) for the beam configuration.

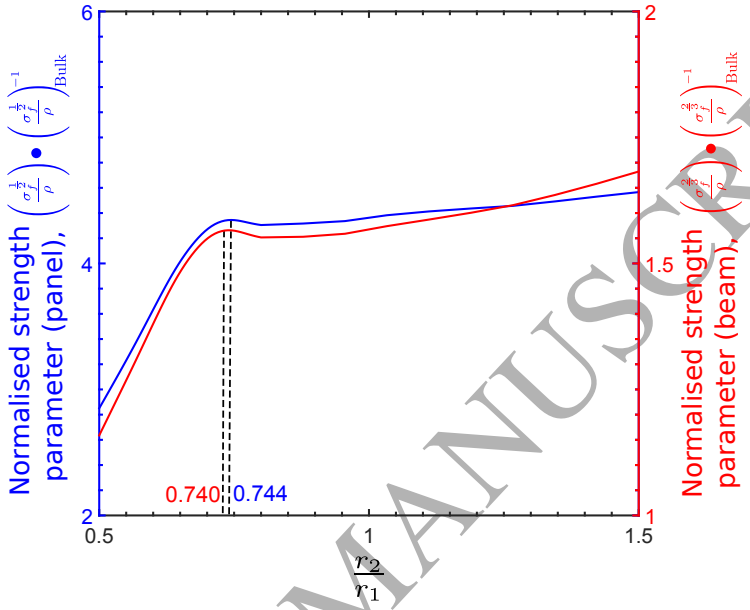

Figure 8: Normalised strength parameter versus $\frac{r_2}{r_1}$ for the BCC lattice.

3.3. Face-centred cubic (FCC)

Fig. 9 and Fig. 10 show the normalised stiffness and strength parameters for the FCC lattice for the panel and beam configurations respectively. The overall trends for the FCC observed in Fig. 9 and Fig. 10 appear to be identical to the trends for the BCC lattice structure observed in Fig. 6 and Fig. 7. The only exception is that the normalised strength parameter for buckling of the FCC lattice being less sensitive to the values of $\frac{r_2}{r_1}$, especially for low values of $\frac{r_2}{r_1}$ compared to the BCC lattice.

Therefore, the intersection between the surfaces for yielding and buckling is also less sensitive to both $\frac{r_2}{r_1}$ and $\frac{r_1}{L_1}$, where the range of $\frac{r_1}{L_1}$ at the intersection, highlighted by the red line in Fig. 9 (b) and Fig. 10 (b), is in between 0.02788 and 0.03000. There were no peaks observed in the normalised strength parameter for both the panel and beam configurations of the FCC structure in Fig. 11, unlike the case for the BCC lattice. The normalised strength parameter in Fig. 11 was found to increase with $\frac{r_2}{r_1}$ throughout the entire range that was studied. Therefore, $\frac{r_2}{r_1}$ should be maximised in order to obtain the optimal strength constrained panel and beams with the FCC structure.

3.4. Regular Octet

The normalised stiffness and strength parameters for the octet lattice are shown in Fig. 12 and Fig. 13 for the panel and beam configurations respectively. As seen in Fig. 12 (a) and Fig. 13 (a), the stiffness parameters for the panel and beam configurations showed identical trends to the BCC and FCC lattice structures described earlier. Conversely, the regular octet lattices' normalised strength parameter for buckling is significantly larger than that for yielding over the entire range of geometric parameters studied. Therefore,

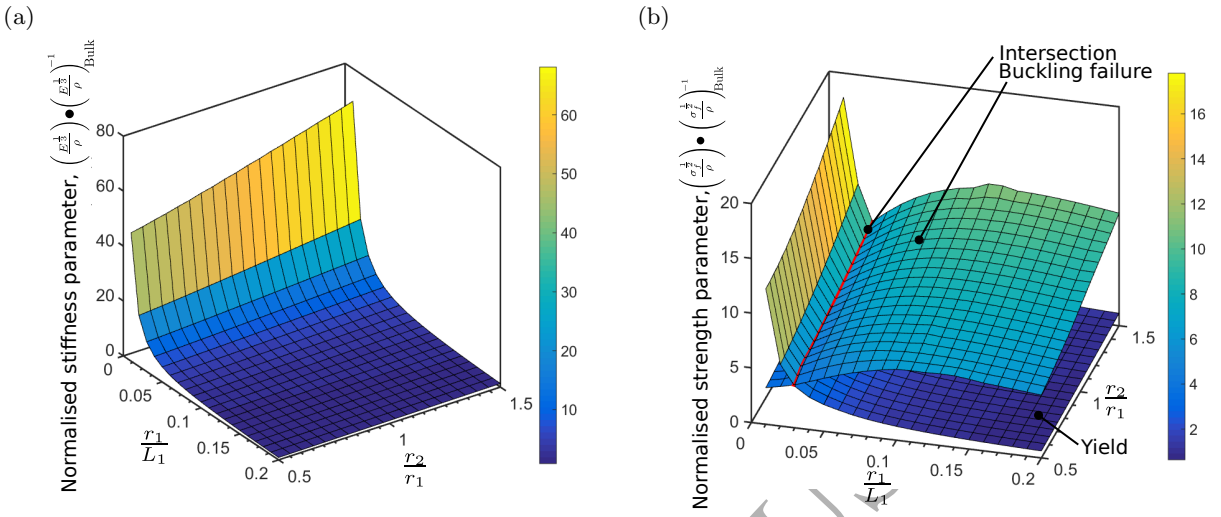

Figure 9: Static properties of the FCC structure with different radii for panel configurations (a) Normalised stiffness parameter (b) Normalised strength parameter.

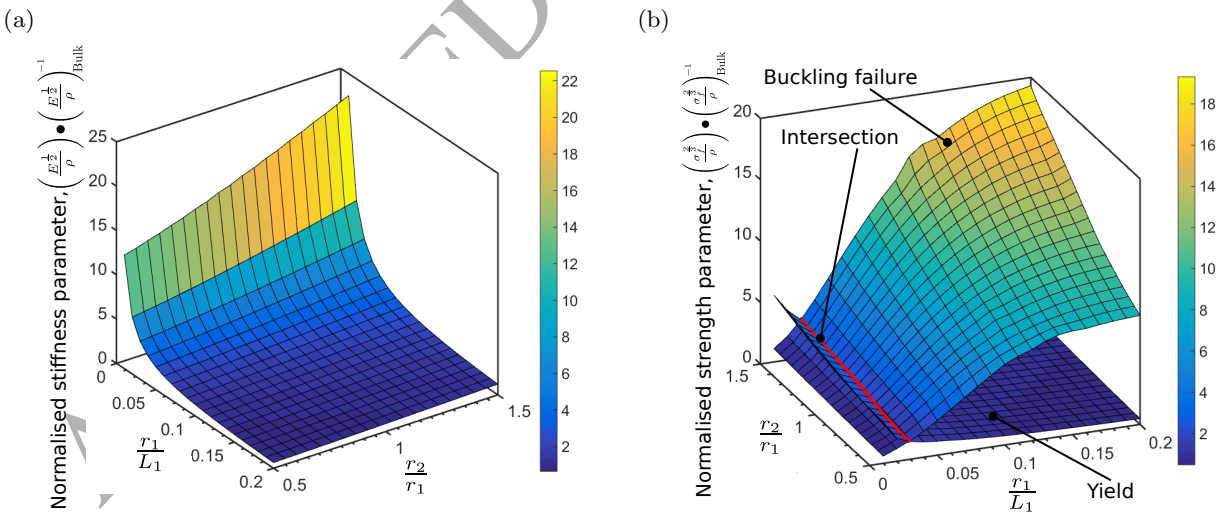

Figure 10: Static properties of the FCC with different radii for beam configurations (a) Normalised stiffness parameter (b) Normalised strength parameter.

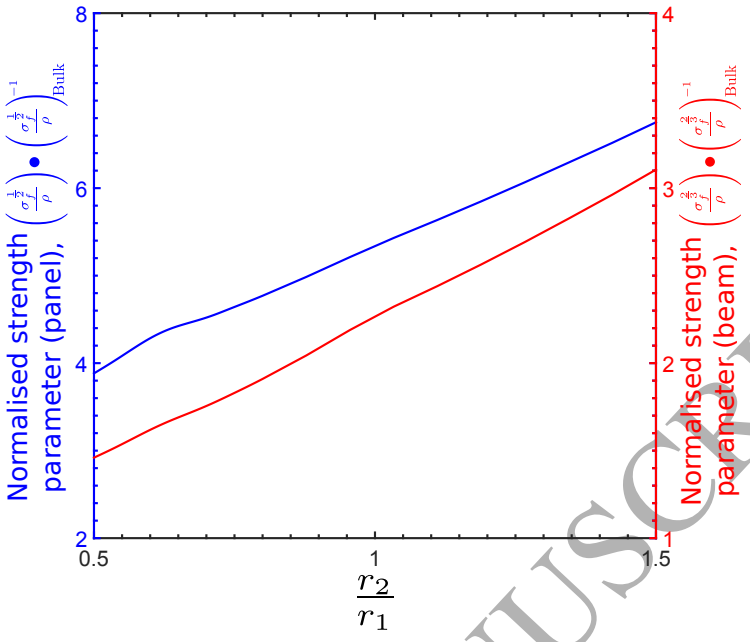

Figure 11: Normalised strength parameter versus $\frac{r_2}{r_1}$ for FCC lattice.

the normalised strength parameter for buckling was not plotted in Fig. 12 (b) and Fig. 13 (b). This result suggests that the octet truss will only fail by yielding and not through buckling. Based on these observations, the optimal regular octet truss geometries in both panel and beam configurations with strength constrains is to minimise $\frac{r_1}{L_1}$ and maximise $\frac{r_2}{r_1}$, with decreasing $\frac{r_1}{L_1}$ having a larger effect.

3.5. General discussion of the static properties of the lattice structures

The mechanical properties of the cubic topologies have been presented in this section. The normalised stiffness and strength parameters for each cases were then compared in order to determine the best topology that gives the optimal static parameters for each case. Table 4 and Table 5 summarise the values and optimal geometric parameters for each geometry. The normalised parameters in Table 4 and Table 5 are ratio of the parameters for the lattices divided to that of the bulk material and are dimensionless.

The optimal geometries of all four cubic topologies for the panel and beam configurations are listed in Table 4 and Table 5 respectively, in which the best topology for a given configuration are bold in the tables. Additionally, for cases in which the parameters for $\frac{r_1}{L_1}$ is to be minimised, this value have been set to 0.01, which will give $r_1 = 1$ mm when $L_1 = 50$ mm. This value is a typical limit based on the resolutions of 3D printers. On the other hand, for values of $\frac{r_2}{r_1}$ that needs to be maximised, these values have been set to 1.5, which is the maximum value studied in this paper.

According to the findings in Table 4 and Table 5, the optimal topology for the panel with stiffness and strength constrains are the simple cubic and octet truss respectively, while the FCC structure is the optimal topology for the beam configuration with both stiffness and strength constrains. An important point to note here is that the analysis done for these topologies are for the uniaxial loading conditions only as the stresses in a beam and panel bending conditions were assumed to be purely axial similar to an Euler-Bernoulli beam or a plate. The analysis with other loading conditions will be too large and is a subject of future work.

4. Band gaps in optimal lattice structure

Resonators were then introduced to the optimal lattice topologies for each configuration from the previous section to produce elastic band gaps. In this study, the target frequency was set to 500 Hz and resonators

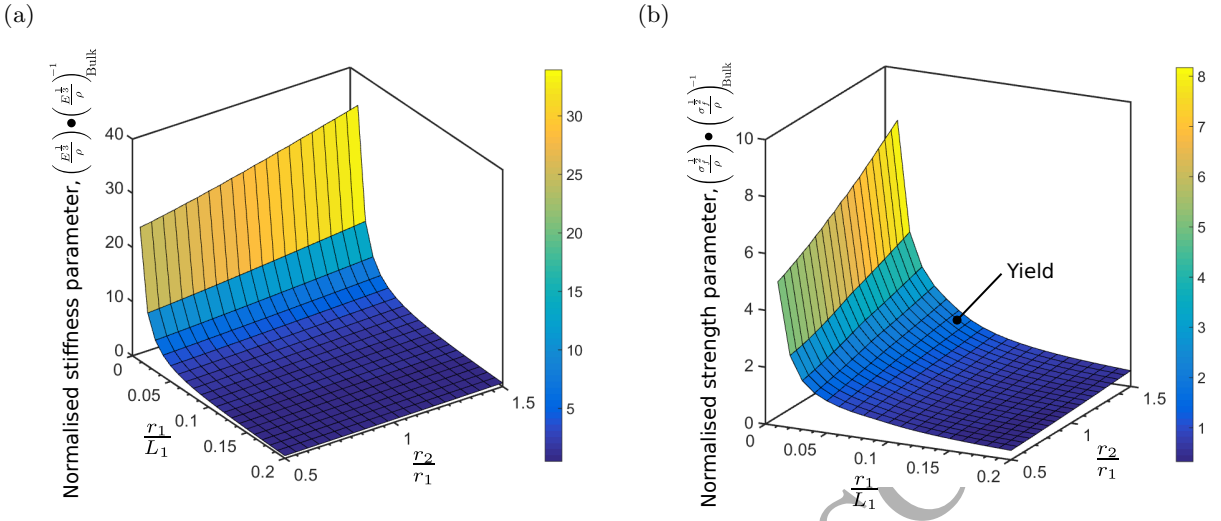

Figure 12: Static properties of the regular octet structure with different radii for panel configurations (a) Normalised stiffness parameter (b) Normalised strength parameter.

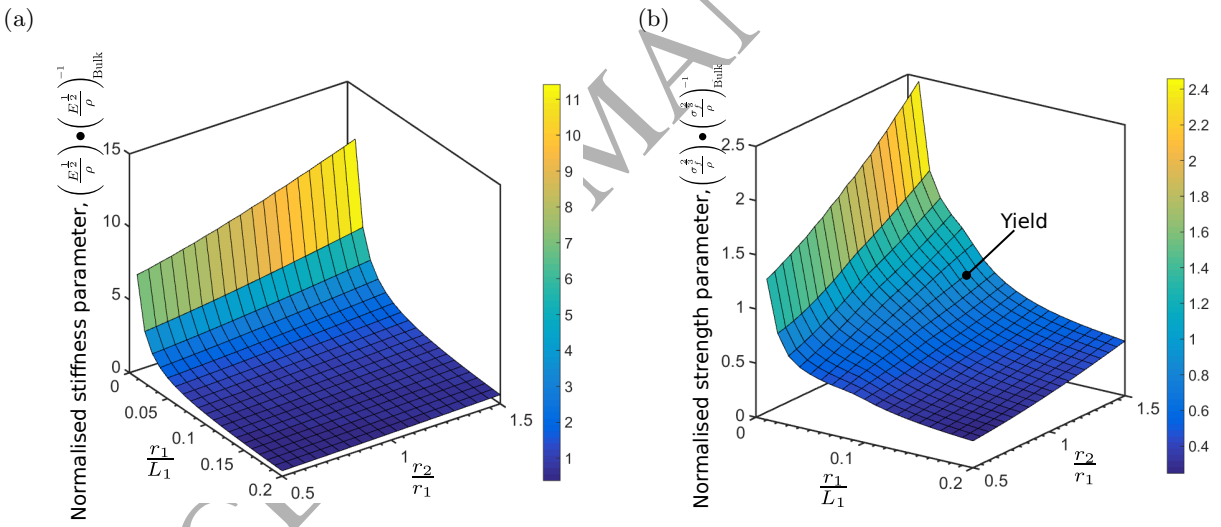

Figure 13: Static properties of the regular octet structure with different radii for beam configurations (a) Normalised stiffness parameter (b) Normalised strength parameter.

Topology	Stiffness Constrained			Strength Constrained		
	$\frac{r_1}{L_1}$	$\frac{r_2}{r_1}$	Normalised Parameter	$\frac{r_1}{L_1}$	$\frac{r_2}{r_1}$	Normalised Parameter
Simple	**0.010**	**N.A.**	**72.13**	0.026	N.A.	7.23
BCC	0.010	1.50	63.95	0.0269	0.744	4.345
FCC	0.010	1.50	68.10	0.02992	1.50	6.774
Octet	0.010	1.50	33.93	**0.010**	**1.50**	**8.172**

Table 4: Optimal normalised parameters for cubic topologies studied (Panel Configuration).

Topology	Stiffness Constrained			Strength Constrained		
	$\frac{r_1}{L_1}$	$\frac{r_2}{r_1}$	Normalised Parameter	$\frac{r_1}{L_1}$	$\frac{r_2}{r_1}$	Normalised Parameter
Simple	0.010	N.A.	18.81	0.026	N.A.	2.591
BCC	0.010	1.50	19.72	0.0269	0.740	1.566
FCC	**0.010**	**1.50**	**22.54**	**0.02992**	**1.50**	**3.11**
Octet	0.010	1.50	11.41	0.010	1.50	2.459

Table 5: Optimal normalised parameters for cubic topologies studied (Beam Configuration).

of different configurations were studied. The width of the band gap will be used as the primary criterion for evaluating the vibration isolation performance. The band gaps of the lattices are evaluated using band diagrams, which are the frequency versus wave vector plots as seen in Fig. 14. A band gap is a region of frequency where there are no bands within the First Brillouin Zone, meaning that no elastic waves can propagate within that band. Therefore, the band gaps are denoted by regions where there are no curves as seen in the highlighted region Fig. 14.

Due to the large number of resonator configurations that were evaluated, a low number of 10 elements per unit strut was used in the band gap calculations to conserve computing resources. Despite the low number of elements, there are no significant differences between the band structure of the case with 22 elements and 10 elements per strut at the range of frequencies of interest, as shown in Fig. 14. Therefore, the errors associated with reducing the mesh fineness will not significantly affect the analysis. The band gaps for the different configurations of every optimal lattice structure will be examined in turn.

(a) (b)

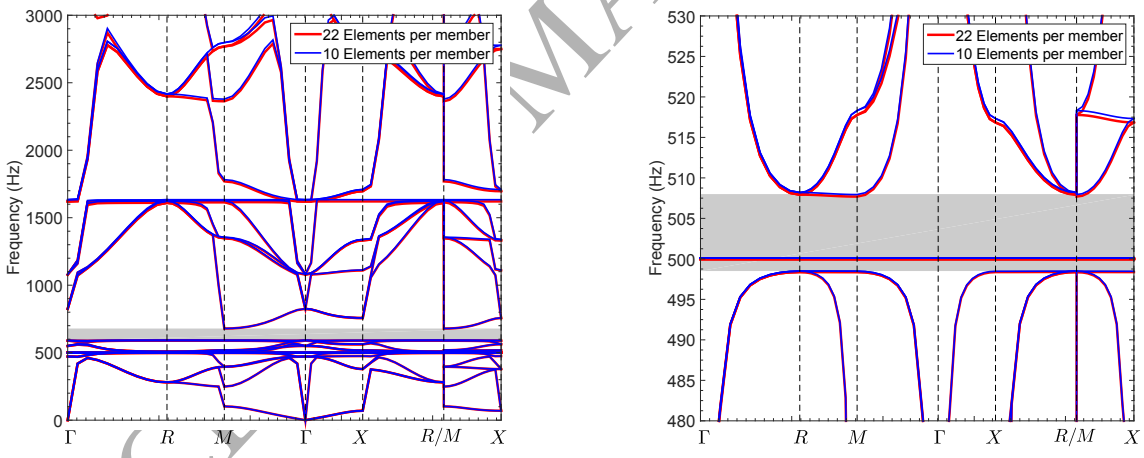

Figure 14: Band structure comparing different mesh density at (a) 0 to 3000 Hz (b) 480 to 530 Hz for the simple cubic lattice with a resonator.

4.1. Optimal lattice for stiffness constrained panel structure (simple cubic lattice)

The optimal lattice topology for the stiffness constrained plate structure is a simple cubic structure. The band structures with and without the resonators are shown in Fig. 15. As seen in Fig. 15 (a), the introduction of the resonators tuned at 500 Hz generated band gaps at 495.2 to 560.9 Hz and 591.0 to 754.8 Hz, which were not present in the case without the resonators. Additionally, a pass band within the band gap region at the tuned frequency of 500 Hz was also observed in Fig. 15 (b). The pass band at the tuned frequency of the local resonators are typical for band gaps produced via the local resonance (LR) phenomenon.

(a) (b)

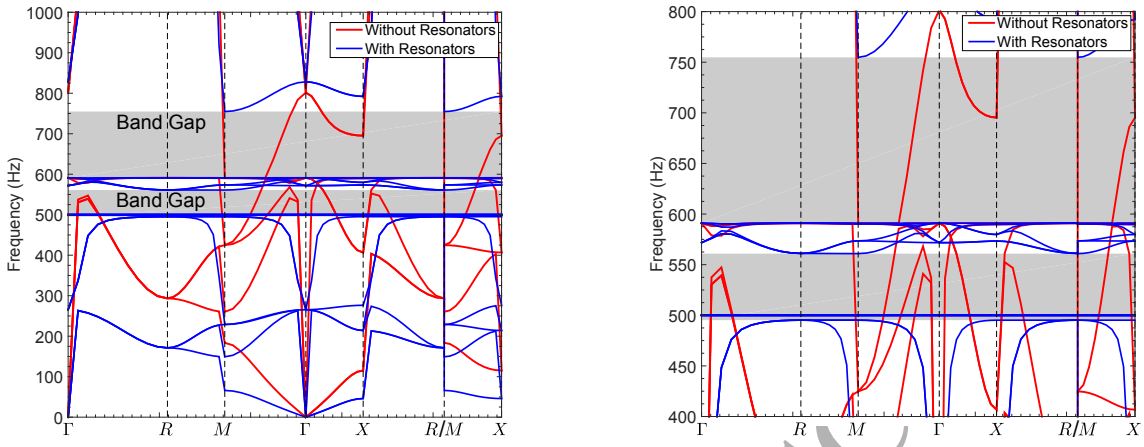

Figure 15: Band structures of simple cubic lattice studied with and without local resonators (a) 0 to 1000 Hz (b) 400 to 800 Hz.

The boundaries of the first band gap for this topology are plotted in Fig. 16 (a) for different values of lengths and radii of the resonators. Only the first band gap will be investigated because it is the only band gap that is directly associated with the tuned frequencies of the resonators. As seen in the figure, the pass band at the tuned frequency of 500 Hz will always be present across all values of lengths and radii. Further observations can be made from Fig. 16 (a). Firstly, the upper bound of the frequency increases with increasing $\frac{r_{\text{Osc}}}{r_1}$ and decreasing $\frac{L_{\text{Osc}}}{L_1}$. On the other hand, the lower bound of the frequency decreases steeply with increasing $\frac{r_{\text{Osc}}}{r_1}$ and decreasing $\frac{L_{\text{Osc}}}{L_1}$. Hence, as illustrated by Fig. 16 (b) that shows the width of the band gaps, the width increases with $\frac{r_{\text{Osc}}}{r_1}$ and decreases $\frac{L_{\text{Osc}}}{L_1}$. Based on these observation, the optimal oscillators should have maximum $\frac{r_{\text{Osc}}}{r_1}$ and minimum $\frac{L_{\text{Osc}}}{L_1}$, so that the width of the band gap is maximised.

However, in order to achieve the same tuned frequency, which is the natural frequency of the resonators, increasing the values of $\frac{r_{\text{Osc}}}{r_1}$ and decreasing $\frac{L_{\text{Osc}}}{L_1}$ will lead to an increase in the mass required for the resonators. This is because the increase in $\frac{r_{\text{Osc}}}{r_1}$ and decrease in $\frac{L_{\text{Osc}}}{L_1}$ will result in a stiffer beam for the resonator and an increase in mass is needed to maintain the same natural frequency. This can be seen in Fig. 17, that shows the density increment, defined as the ratio of the increase in density to the original density of the lattice, for different geometries of the resonator beams. The required mass increases exponentially with increasing $\frac{r_{\text{Osc}}}{r_1}$ and decreasing $\frac{L_{\text{Osc}}}{L_1}$. This suggests that the increase in band gap width will also result in an increase in density of the lattice, which is undesirable for light-weight applications.

As seen in Table 1, the parameters to be maximised are directly proportional to the inverse of density. Therefore, the increase in mass can still be justified if these parameters multiplied by (1+ Density increment), described by Eq. (16), is still significantly larger than unity. This is because the static properties for light-weight structural applications after the addition of the resonators are still better than the bulk material.

$$P_{\text{With resonators}} = \frac{P_{\text{Without resonators}}}{(1 + \text{Density Increment})} \tag{16}$$

where P is the parameter shown in Table 1.

Since the optimal parameter for the simple cubic case is 72.13, as shown in Table 4, it is likely that this is possible. For example, an overlap of the contour plot of the density increment (the red lines) and the width of the band gaps (the other lines) in Fig. 18 (a), shows that band gaps of more than 20 Hz is achievable, where the static parameter after adding the resonators is still larger than 10, although a mass of 5 times the original lattice is added to the system.

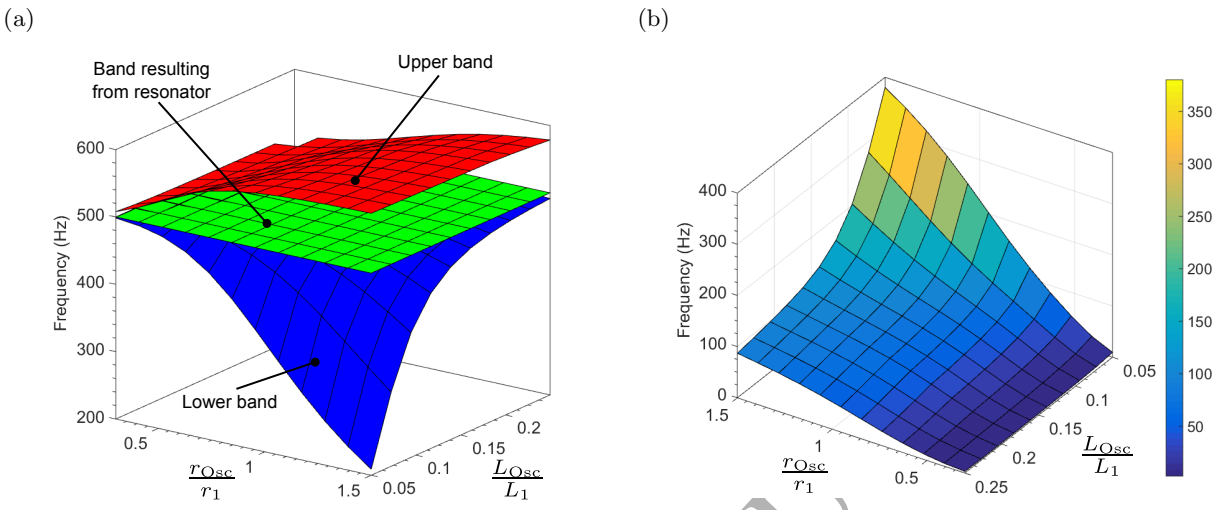

Figure 16: (a) Upper and lower bounds of the first band gaps (b) width of first band gap for different resonator configurations for simple cubic structure.

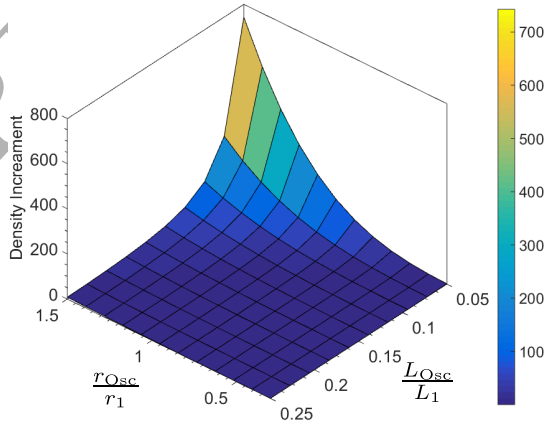

Figure 17: Density increment with the addition of resonators for simple cubic lattice.

Furthermore, the band gap width per unit density increment contour plot, as shown in Fig. 18 (b), was studied to determine the beam configuration that will give the maximum band gap width while minimising the penalty of increasing density. As seen in Fig. 18 (b), there is a peak at approximately $\frac{L_{\text{Osc}}}{L_1} = 0.2$ and $\frac{r_{\text{Osc}}}{r_1} = 0.4$ with a value of 50. This result suggests that there is a maximum band gap width per unit density increment for a tuned resonator and optimisation methods can be implemented to find this value.

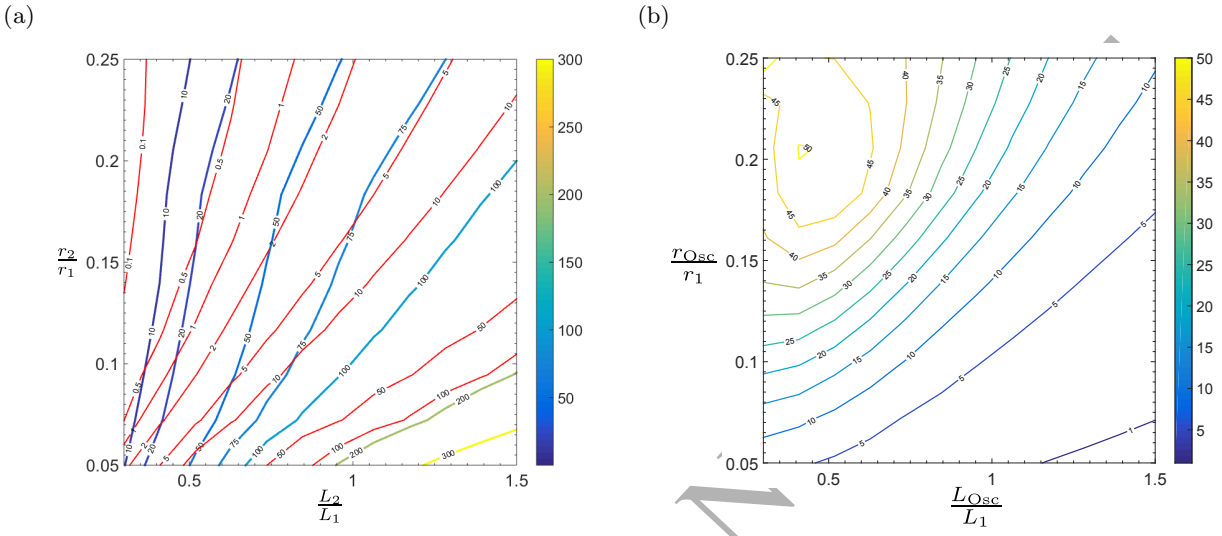

Figure 18: (a) Overlap of density increment and band gap width contour plot, red contour denote density increment while the other contour denotes band gap width (b) Band gap width per unit density increment contour plot for simple cubic structures.

4.2. Optimal lattice for strength constrained panel structure (octet lattice)

The upper and lower bounds of the optimal lattice for the strength constrained plate structure found in Section 3.5 are plotted in Fig. 19 (a). The band structure for this lattice configuration share similar trends with the simple cubic structure discussed in the previous section. It has a pass band for all lengths and radii of the resonators at the tuned frequency of 500 Hz. The trends of the upper and lower bounds of the band gap, and subsequently the band gap width with respect to $\frac{r_{\text{Osc}}}{r_1}$ and $\frac{L_{\text{Osc}}}{L_1}$ follow the same trends as the ones for the simple cubic structure.

The trends of the density increment resulting from the addition of the resonators for this lattice configuration are similar to the simple cubic structure. The similar trends of this lattice and the simple cubic structure is expected because the same mechanism was used to produce the band gaps. Since the trends in density increment are similar for all lattices for the same reasons, the density increments will not be plotted herein but are available in the supplementary material for this paper.

The density increment for the regular octet structure is lower due to the larger original density of the unit cell. Although the density increment from the addition of the resonators is lower for the octet structure, the band gap width per unit density increment for the octet lattice, shown in Fig. 20 (b), is significantly lower than that for the simple cubic structure in Fig. 18 (b). The cause of this is the significantly smaller band gap width produced by the resonators as shown in Fig. 20 (a). This result suggests that there is a positive correlation between the mass of the oscillators and the width of the band gap. Furthermore, no distinct peak was observed in Fig. 20 (b), although it appears to have a region with relatively high values and the maximum appears to be outside the range that was investigated.

4.3. Optimal lattice for stiffness constrained beam structure (FCC lattice)

The optimal lattice structure for a stiffness constrained beam structure, which has an FCC topology, has a band gap from 411.3 to 485.6 Hz, as seen in Fig. 21, even though no local resonators were present. The

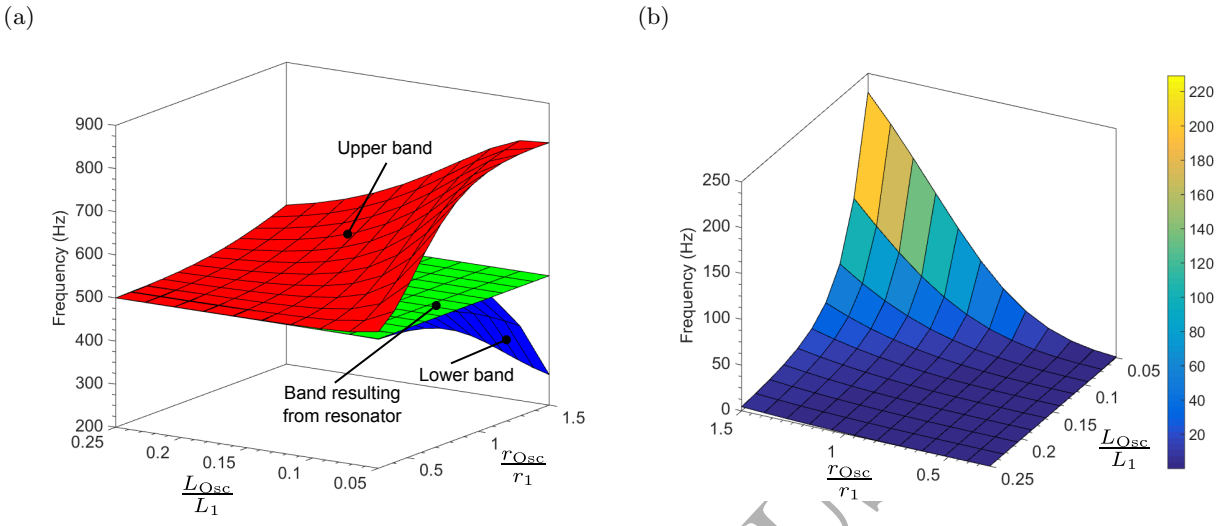

Figure 19: (a) Upper and lower bounds of the first band gaps (b) width of first band gap for different resonator configurations for the regular octet lattice.

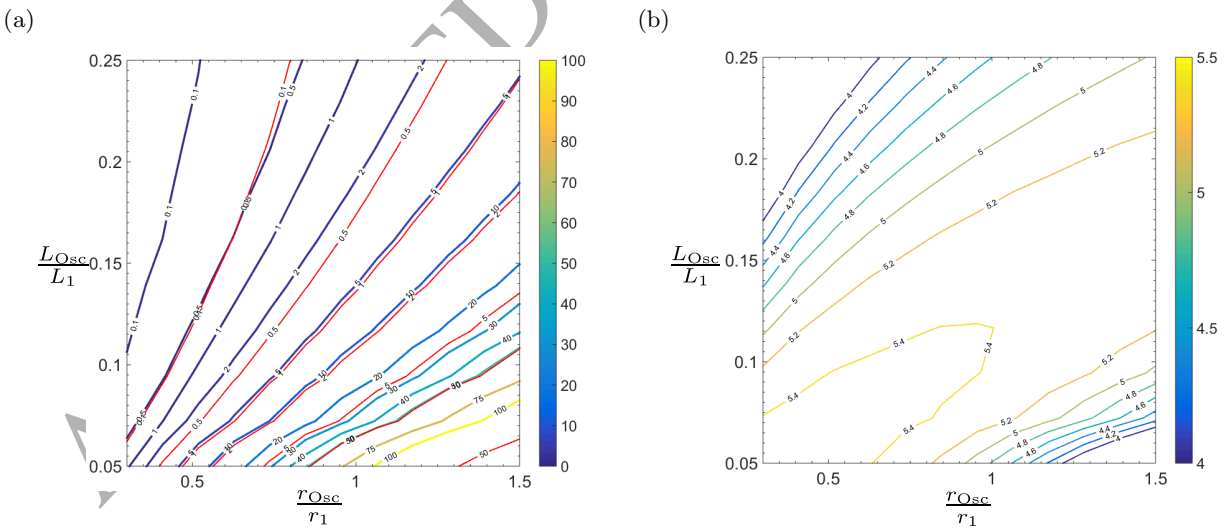

Figure 20: (a) Overlap of density increment and band gap width contour plot, red contour denote density increment while the other contour denotes band gap width (b) Band gap width per unit density increment contour plot for the regular octet lattice.

band gap without the local resonators will be referred to as the original gap herein, while the band gap with the resonators will be referred to as the resonator gap.

(a) (b)

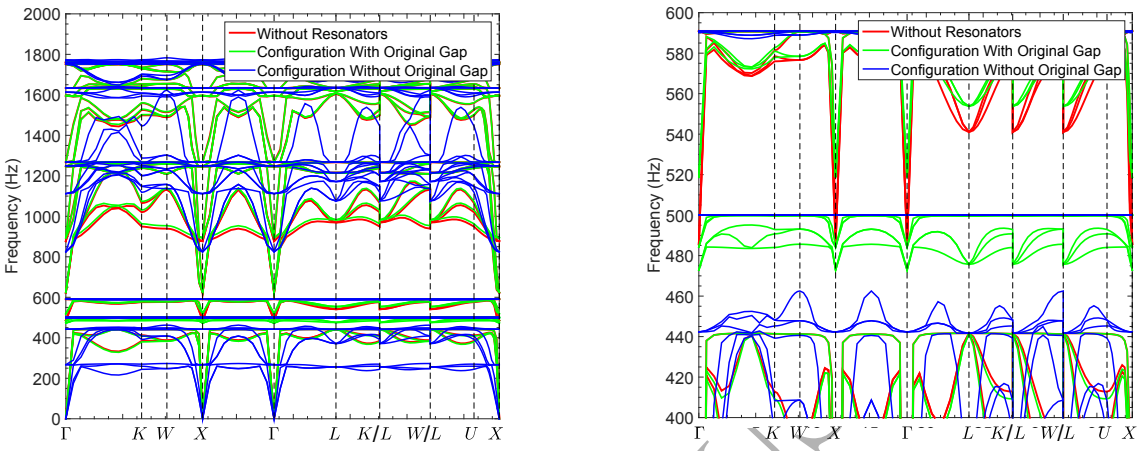

Figure 21: Band structures of FCC studied with and without local resonators (a) 0 to 2000 Hz (b) 400 to 600 Hz.

The upper and lower bounds of the resonator gap and the original gap are shown in Fig. 22 (a), while the band gap widths are shown in Fig. 22 (b). As expected, the general trend for the upper and lower bounds, the band gap widths, and density increment of the resonator gap are similar to the previous structures.

However, the addition of the resonators affects the original gap. Firstly, the introduction of the resonators results in a reduction in the width of the original gap. Furthermore, the original gap appears to have the opposite trend of the resonator gap, as seen in Fig. 22 (a) and (b), where the original gap's width decreases with increasing $\frac{r_{\mathrm{Osc}}}{r_1}$ and decreasing $\frac{L_{\mathrm{Osc}}}{L_1}$ until it eventually closes. Increasing the width of the resonator gap will lead to a decrease in the original gap.

(a) (b)

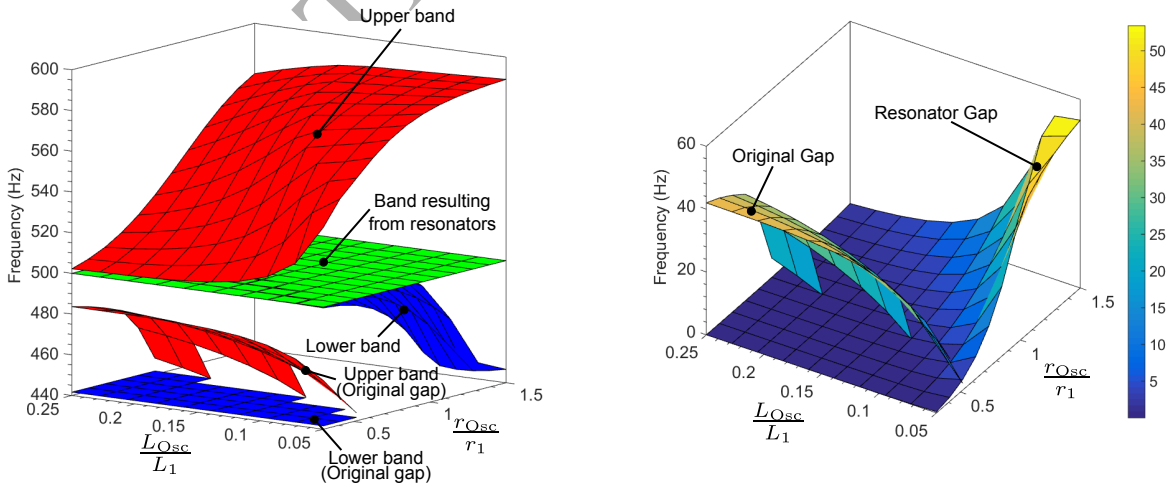

Figure 22: (a) Upper and lower bounds of the first band gaps (b) width of first band gap for different resonator configurations for the FCC structure.

Additionally, some differences in the band structure were observed for the case when the original gap is present, as seen in Fig. 21. When the influence of the resonator gap is low, the band structure of the lattice is similar to the case without the resonators. The resonators generate a pass band at a frequency slightly lower than the tuned frequency, while creating an additional band gap above 500 Hz. On the other hand, when the effects of the resonators become significant, the band structure with the resonators differs significantly from the original case, this can be seen by comparing the green and blue curve shown in Fig. 21.

The overlap of the band gap width contour plot and the density increment from the addition of the resonators are shown in Fig. 23 (a) and (b) for the original gap and the resonator gap respectively. As seen in Fig. 23 (a), the band gap width of the original gap appears to be reducing with density increment, contrary to the observation made in Fig. 23 (b) for the resonator gap. There are no contours for the band gap width for the original gap at higher $\frac{r_{\text{Osc}}}{r_1}$ as the original gap closes. This observation is analogous to the original gap being "*cannibalised*" by the larger resonator gap when resonators with larger masses are used. Unfortunately, for this configuration, the band gap width resulting from the addition of the resonators is relatively low. For example, based on Fig. 23 (b), the added resonators will result in an increase of 5 times the density of the lattice to achieve a 10 Hz band gap. This significantly reduces the original parameter from 22.54 to 3.75. The significant reduction in the stiffness parameter means the strategy of adding resonators may not be suitable for this configuration.

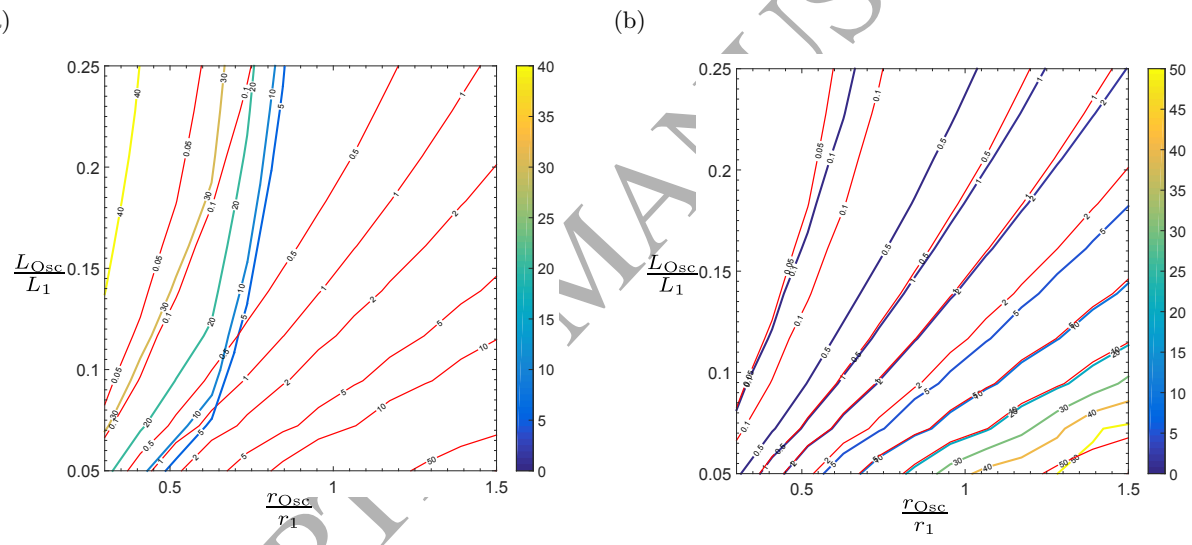

Figure 23: Overlap of density increment and band gap width contour plot, red contour denote density increment while the other contour denotes band gap width (a) Original gap (b) Resonator gap for the FCC lattice.

The band gap width per unit density increment for the original and resonator gaps are shown in Fig. 24 (a) and (b) respectively. As expected, the trend observed for the resonator gap in Fig. 24 (b) is similar to that for the octet truss discussed previously. However, compared to the other lattice configurations, the band gap width per unit density increment for this FCC configuration, seen in Fig. 24 (b), is significantly lower than the other lattice configurations, especially the simple cubic configuration. This result suggests that the addition of resonator does not provide large band gap widths for the increase in mass. However, by comparing Fig. 24 (a) and (b), the band gap width per unit density increment for the orginal gap is approximately three orders of magnitude higher than that for the resonator gap. This result indicates that the original gap strategy should be pursued in favour of the addition of resonators if these gaps are present around the desired frequencies as this does not increase the lattice density.

4.4. Optimal lattice for strength constrained beam structure (FCC lattice)

The final configuration is the FCC lattice that has the optimal geometrical parameters for a strength constrained beam structure. The upper and lower bounds of the first band gap for this lattice topology and

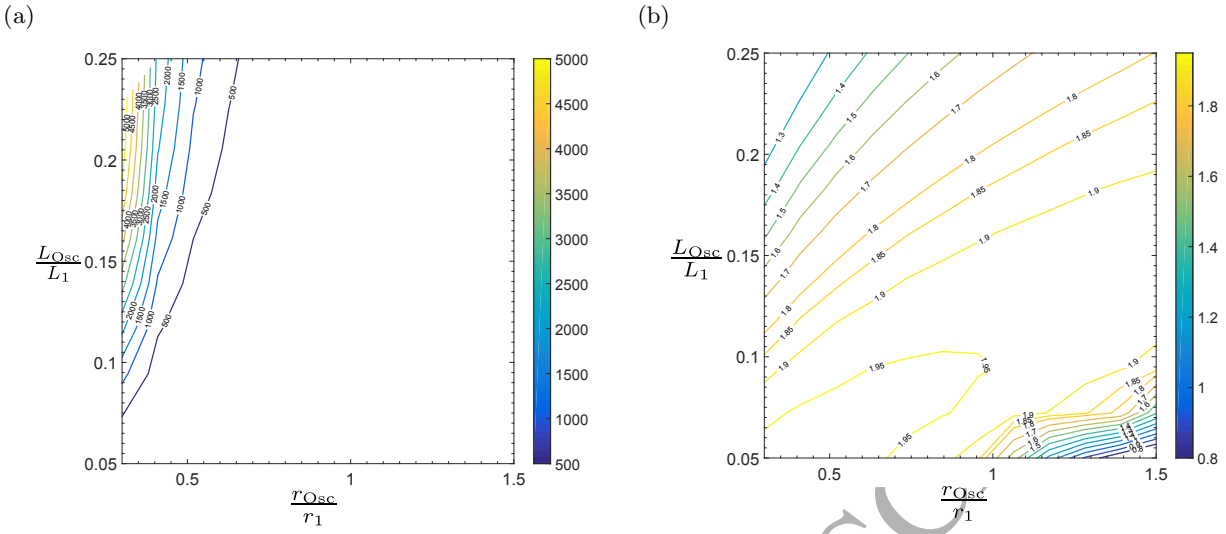

Figure 24: Band gap width per unit density increment contour plot (a) Original gap (b) Resonator gap for the FCC lattice.

the width of the first band gap are shown in Fig. 25 (a) and (b) respectively. As seen in Fig. 25 (a), there is an additional band gap at low values of $\frac{L_{Osc}}{L_1} = 0.05$. This band gap will not be investigated as the band gap of interest is the one related to the tuned frequency of 500 Hz. Additionally, unlike the previous FCC case, there are no band gaps present for this case when no resonators are added. Similar to the other lattice structures being investigated, the band gap follows the trends observed in the other lattices.

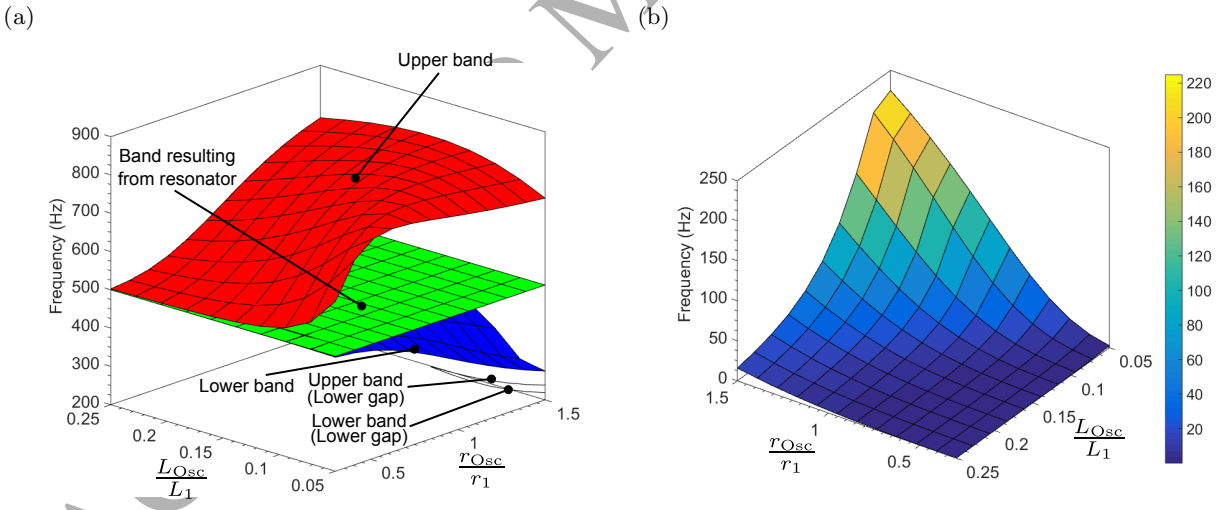

Figure 25: (a) Upper and lower bounds of the first band gaps (b) width of first band gap for different resonator configurations for the FCC lattice.

The overlap of the band gap width contour plot and the density increment from the addition of the resonators are shown in Fig. 26 (a) and (b) respectively. Again, the observed trends are similar to other configurations. However, the optimal band gap width per unit density increment for this structure appears to be outside the range of values being studied. Lastly, the band gap width per unit density increment, shown in Fig. 26 (b), also suggests that the resonators that were added are not efficient in generating the

band gaps. This is undesirable, especially when the normalised strength parameter is already low at 3.11. A further investigation of Fig. 26 (a) shows that in order to produce a band gap with a width of 5 Hz, the added mass will result in a density increment of 10 times the original density. This will lead to the parameter with the oscillators being reduced to 0.2828 which is significantly lower than that for the bulk material. Hence, the strategy of adding resonators is not a viable option for this case.

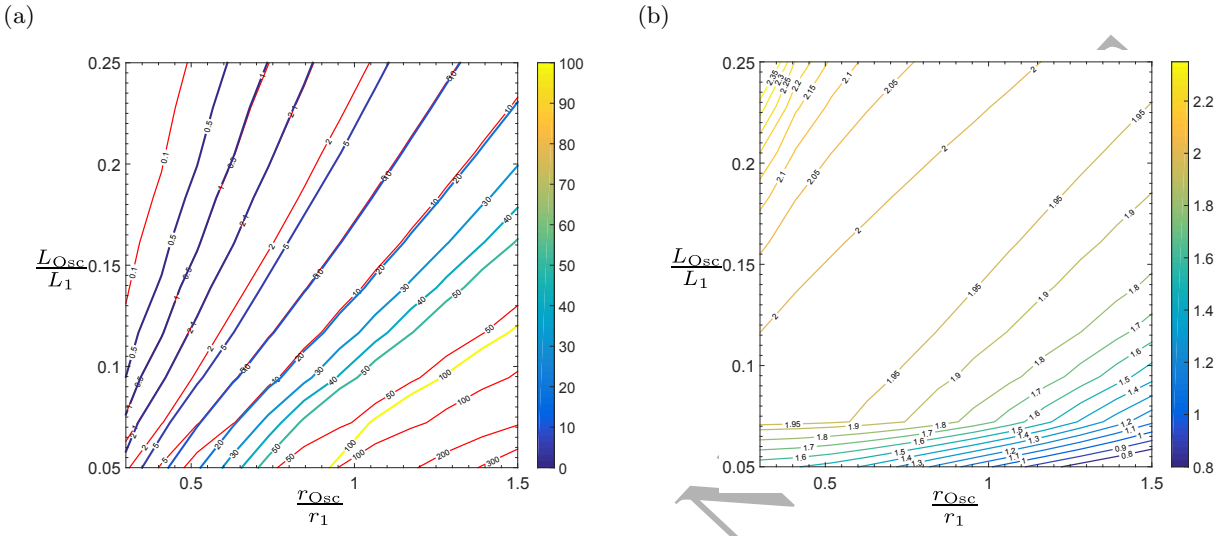

Figure 26: (a) Overlap of density increment and band gap width contour plot, red contour denote density increment while the other contour denotes band gap width (b) Band gap width per unit density increment contour plot for the FCC lattice.

4.5. General discussion on band gap behaviour of lattice with oscillators

Local resonators were added to the lattice structures with the optimal static properties from Section 3.5 in order to produce locally resonant (LR) band gaps. This method is similar to the method employed in [15]. The location of the band gaps were tuned to be 500 Hz and resonators of different lengths, radii, and mass were studied. Although the band gaps were tuned to be 500 Hz in this study, the general trends of the band gaps should be similar for resonators with other frequencies, with the differences being the location of the optimal band gap width per unit density being at different values of length and radius. The procedure introduced in this study can be used to determined the trends for resonators with other tuned frequencies.

The LR gaps produced by the addition of the resonators all showed similar trends, in which the band gap width increases with increasing $\frac{r_{Osc}}{r_1}$ and decreasing $\frac{L_{Osc}}{L_1}$. However, the increase in the LR band gap width comes at a cost of an increase in the density, suggesting a positive correlation between the band gap width and the resonator mass. For cases where the static parameters are significantly better than the bulk material, such as the simple cubic and FCC lattices for the plate configurations, the normalised stiffness and strength parameters after adding the resonators may still be significantly higher than the bulk material despite the increase in density. Conversely, for other cases especially where the static parameters are only marginally better than the bulk material, for example the FCC and octet structures for the beam configurations, the parameter may reduce below that for the bulk material and the strategy of adding local resonators is not viable. Hence, the increase in density is a key consideration when employing the strategy outlined in this paper to produce multifunctional lightweight structural materials with elastic band gap properties.

Additionally, some lattice structures, such as one of the FCC lattice investigated here, have band gaps prior to the introduction of the resonators. These band gaps have far larger widths compared to that introduced by the resonators and do not come with a penalty on the density. Therefore, tuning the original band gap to the desired frequency is a more favourable solution to the addition of the local resonators

when these band gaps are present. This result suggests that other techniques, such as manipulating the connectivity of the struts in [27] are worthy for further study for multi-purpose applications.

There are several improvements that can be made to increase the band gap widths that can be studied further. One possible improvement is to design hybrid 3D cores, where two or more topologies are combined in a spatially periodic pattern that may increase the band gap width. Another possible strategy is to arrange the unit cells with different resonators in series with overlapping band gaps. This may result in a very wide band gap to effectively attenuate vibrations, for example as seen in [13]. Lastly, as in beam or panel configurations, the axial length is generally larger than the width or height of the system. Therefore, there is a potential to improve the band gap and static performance of the lattice structure by varying the width and height independently. These possible improvements are topics of future study in this field.

5. Summary and Conclusions

Lattice structures have huge potential for multifunctional applications. In this paper, a parametric study was conducted in order to investigate the viability of cubic structures to be used as both a lightweight structural component with vibration isolation properties. The stiffness and strength properties of four different cubic lattice topologies, made from ABS, to be used as core materials for sandwich beams and panels were investigated in order to determine the best topology and geometric parameters. In general, the normalised stiffness parameter was found to increase with the radii of the member struts for all topologies. The strength of the lattice topologies were determined by two failure mechanism, which are yielding and buckling of the struts. The yielding parameter increases with increasing $\frac{r_2}{r_1}$ and decreases with increasing $\frac{r_1}{L_1}$, for all the topologies except the simple cubic lattice that has no diagonal struts. On the other hand, the normalised strength parameter for buckling increases with increasing $\frac{r_2}{r_1}$ and increasing $\frac{r_1}{L_1}$ for all topologies with the exception of the octet truss, which does not experience buckling. The failure strength of the topologies was set to be the lower of the yielding and buckling failure modes. Therefore, the optimal topology for the strength was found to be the point in which the yield and buckling criteria are equal. The lattice topologies were found to be able to have superior static mechanical properties compared to that of the parent bulk material. Based on these findings, the optimal topology for each configuration was found.

After that, tuned resonators made from cantilever beams with masses at the end were added to the topologies to introduce band gaps via the local resonance mechanism. The resonators were tuned to have a natural frequency of 500 Hz. Since there are different parameters, such as the lengths, radii, and added mass, which can produce resonators of a given natural frequency, the effects of these geometrical parameters on the band gap widths were also studied. For all topologies, the band gap width produced by the introduction of the resonators follow the same trend. The band gap width was found to be larger for increasing values of $\frac{r_{\mathrm{Osc}}}{r_1}$ and decreasing values of $\frac{L_2}{L_1}$ but this is accompanied by an increase in density. This is because the required changes to increase the band gap width will result in a stiffer beam and a larger mass is required to give the same natural frequency. With the increase of density resulting from the introduction of the oscillators, the strength and stiffness parameters for the lattice structures reduces. Based on the findings of this investigation, the addition of the resonators is justifiable if the stiffness or strength parameter is still significantly larger than that for the bulk material, as seen in some of the topologies investigated here. However, for other cases, such as the FCC for the strength constrained beam structure, the value falls below that for the bulk material and this strategy is not viable. Therefore, the increase in density and the decrease in the normalised stiffness and strength parameter are important factors to consider when adding resonators to such structural components to introduce elastic band gaps.

Lastly, some topologies such as one of the FCC topology studied here have a band gap prior to the addition of the resonators. Since the addition of the resonators will only degrade the original gap, the best strategy is to make changes to the structure to achieve the desired band gap frequency because the original gap does not result in the addition of mass.

Acknowledgements

The strong support from The Aviation Industry Corporation of China (AVIC), First Aircraft Institute (FAI) and Beijing Aeronautical Manufacturing Technology Research Institute (BAMTRI) for this funded research is much appreciated. The research was performed at the AVIC Centre for Structural Design and Manufacture at Imperial College London.

References

[1] V. Deshpande, N. Fleck, M. Ashby, Effective properties of the octet-truss lattice material, Journal of the Mechanics and Physics of Solids 49 (2001) 1747–1769.
URL http://www.sciencedirect.com/science/article/pii/S0022509601000102

[2] N. Fleck, V. Deshpande, M. Ashby, Micro-architectured materials: past, present and future, Proceedings of the Royal Society A: Mathematical, Physical and Engineering Sciences 466 (2121) (2010) 2495–2516. doi:10.1098/rspa.2010.0215.
URL http://rspa.royalsocietypublishing.org/cgi/doi/10.1098/rspa.2010.0215

[3] C. A. Steeves, C. Mercer, E. Antinucci, M. Y. He, A. G. Evans, Experimental investigation of the thermal properties of tailored expansion lattices, International Journal of Mechanics and Materials in Design 5 (2) (2009) 195–202. doi:10.1007/s10999-009-9094-6.
URL http://www.springerlink.com/index/10.1007/s10999-009-9094-6

[4] C. A. Steeves, S. L. dos Santos e Lucato, M. He, E. Antinucci, J. W. Hutchinson, A. G. Evans, Concepts for structurally robust materials that combine low thermal expansion with high stiffness, Journal of the Mechanics and Physics of Solids 55 (9) (2007) 1803–1822. doi:10.1016/j.jmps.2007.02.009.
URL http://linkinghub.elsevier.com/retrieve/pii/S0022509607000385

[5] J. Berger, C. Mercer, R. M. McMeeking, A. G. Evans, The Design of Bonded Bimaterial Lattices that Combine Low Thermal Expansion with High Stiffness, Journal of the American Ceramic Society 94 (2011) S42–S54. doi:10.1111/j.1551-2916.2011.04503.x.
URL http://doi.wiley.com/10.1111/j.1551-2916.2011.04503.x

[6] M. J. Leamy, Exact wave-based Bloch analysis procedure for investigating wave propagation in two-dimensional periodic lattices, Journal of Sound and Vibration 331 (7) (2012) 1580–1596. doi:10.1016/j.jsv.2011.11.023.
URL http://linkinghub.elsevier.com/retrieve/pii/S0022460X11009011

[7] L. Raghavan, S. Phani, Bandgap formation mechanisms in periodic materials and structures, in: Proceedings of Meetings on Acoustics, Vol. 19, Montreal, 2013, p. 045021. doi:10.1121/1.4799378.
URL http://link.aip.org/link/PMARCW/v19/i1/p045021/s1{&}Agg=doi

[8] A. Phani, J. Woodhouse, N. Fleck, Wave propagation in two-dimensional periodic lattices, The Journal of the Acoustical Society of America 119 (4) (2006) 1995. doi:10.1121/1.2179748.
URL http://link.aip.org/link/JASMAN/v119/i4/p1995/s1{&}Agg=doi

[9] E. Baravelli, M. Carrara, M. Ruzzene, High stiffness, high damping chiral metamaterial assemblies for low-frequency applications, Proc. SPIE 8695, Health Monitoring of Structural and Biological Systems.
URL http://proceedings.spiedigitallibrary.org/proceeding.aspx?articleid=1680001

[10] D. C. Lagoudas, J. J. Mayes, M. M. Khan, Simplified Shape Memory Alloy (SMA) Material Model for Vibration Isolation, Smart Structures and Materials (2001) 452–461doi:10.1117/12.436514.
URL http://proceedings.spiedigitallibrary.org/proceeding.aspx?articleid=907352

[11] M. F. Ashby, The properties of foams and lattices., Philosophical transactions. Series A, Mathematical, physical, and engineering sciences 364 (1838) (2006) 15–30. doi:10.1098/rsta.2005.1678.
URL http://www.ncbi.nlm.nih.gov/pubmed/18272451

[12] M. F. Ashby, A. G. Evans, N. A. Fleck, L. J. Gibson, J. W. Hutchinson, H. N. G. Wadley, Metal Foams: A Design Guide, Butterworth-Heinemann, 2000.

[13] E. Baravelli, M. Ruzzene, Internally resonating lattices for bandgap generation and low-frequency vibration control, Journal of Sound and Vibration 332 (25) (2013) 6562–6579. doi:10.1016/j.jsv.2013.08.014.
URL http://linkinghub.elsevier.com/retrieve/pii/S0022460X13006792

[14] X. Liu, G. Hu, C. Sun, G. Huang, Wave propagation characterization and design of two-dimensional elastic chiral metacomposite, Journal of Sound and Vibration 330 (2011) 2536–2553. doi:10.1016/j.jsv.2010.12.014.
URL http://linkinghub.elsevier.com/retrieve/pii/S0022460X10008278

[15] W. Liu, J. W. Chen, X. Y. Su, Local resonance phononic band gaps in modified two-dimensional lattice materials, Acta Mechanica Sinica 28 (3) (2012) 659–669. doi:10.1007/s10409-012-0031-9.
URL http://link.springer.com/10.1007/s10409-012-0031-9

[16] E. Dragoni, Optimal mechanical design of tetrahedral truss cores for sandwich constructions, Journal of Sandwich Structures and Materials 15 (4) (2013) 464–484. doi:10.1177/1099636213487364.
URL http://jsm.sagepub.com/cgi/doi/10.1177/1099636213487364

[17] J.-E. Choi, G.-D. Ko, K.-J. Kang, Taguchi method-based sensitivity study of design parameters representing specific strength of wire-woven bulk Kagome under compression, Composite Structures 92 (10) (2010) 2547–2553. doi:10.1016/j.compstruct.2010.01.024.
URL http://www.sciencedirect.com/science/article/pii/S026382231000067X

[18] A. Vigliotti, D. Pasini, Stiffness and strength of tridimensional periodic lattices, Computer Methods in Applied Mechanics and Engineering 229 (2012) 27–43. doi:10.1016/j.cma.2012.03.018.
URL http://www.sciencedirect.com/science/article/pii/S0045782512000941

[19] R. A. W. Mines, On the Characterisation of Foam and Micro-lattice Materials used in Sandwich Construction, Strain 44 (1) (2008) 71–83. doi:10.1111/j.1475-1305.2008.00399.x.

[20] J. Wallach, L. Gibson, Mechanical behavior of a three-dimensional truss material, International Journal of Solids and Structures 38 (40-41) (2001) 7181–7196. doi:10.1016/S0020-7683(00)00400-5.
URL http://linkinghub.elsevier.com/retrieve/pii/S0020768300004005

[21] E. Ptochos, G. Labeas, Elastic modulus and Poissons ratio determination of micro-lattice cellular structures by analytical, numerical and homogenisation methods, Journal of Sandwich Structures and Materials 14 (5) (2012) 597–626. doi:10.1177/1099636212444285.
URL http://jsm.sagepub.com/content/14/5/597.abstract

[22] E. Ptochos, G. Labeas, Shear Modulus Determination of Cuboid Metallic Open-Lattice Cellular Structures by Analytical, Numerical and Homogenisation Methods, Strain 48 (5) (2012) 415–429. doi:10.1111/j.1475-1305.2012.00837.x.

[23] Y. L. Xu, C. Q. Chen, X. G. Tian, Wave Characteristics of Two-Dimensional Hierarchical Hexagonal Lattice Structures, Journal of Vibration and Acoustics 136 (1) (2013) 011011. doi:10.1115/1.4025550.
URL http://vibrationacoustics.asmedigitalcollection.asme.org/article.aspx?doi=10.1115/1.4025550

[24] Y. Liu, X. Z. Sun, W. Z. Jiang, Y. Gu, Tuning of Bandgap Structures in Three-Dimensional Kagome-Sphere Lattice, Journal of Vibration and Acoustics 136 (2) (2014) 021016. doi:10.1115/1.4026211.
URL http://vibrationacoustics.asmedigitalcollection.asme.org/article.aspx?doi=10.1115/1.4026211

[25] F. Scarpa, M. Ouisse, M. Collet, K. Saito, Kirigami Auxetic Pyramidal Core: Mechanical Properties and Wave Propagation Analysis in Damped Lattice, Journal of Vibration and Acoustics 135 (4) (2013) 041001. doi:10.1115/1.4024433.
URL http://vibrationacoustics.asmedigitalcollection.asme.org/article.aspx?doi=10.1115/1.4024433

[26] M. I. Hussein, M. J. Leamy, M. Ruzzene, Dynamics of Phononic Materials and Structures: Historical Origins, Recent Progress, and Future Outlook, Applied Mechanics Reviews 66 (4) (2014) 040802. doi:10.1115/1.4026911.
URL http://appliedmechanicsreviews.asmedigitalcollection.asme.org/article.aspx?doi=10.1115/1.4026911

[27] P. Wang, F. Casadei, S. H. Kang, K. Bertoldi, Locally resonant band gaps in periodic beam lattices by tuning connectivity, Physical Review B 020103 (2015) 2–5. doi:10.1103/PhysRevB.91.020103.

[28] M. F. Ashby, Materials Selection in Mechanical Design, 3rd Edition, Butterworth-Heinemann, Burlington, MA, 2005.

[29] S. Shaffer, K. Yang, J. Vargas, M. A. Di Prima, W. Voit, On reducing anisotropy in 3D printed polymers via ionizing radiation, Polymer (United Kingdom) 55 (23) (2014) 5969–5979. doi:10.1016/j.polymer.2014.07.054.
URL http://dx.doi.org/10.1016/j.polymer.2014.07.054

[30] A. Bellini, S. Guceri, Mechanical characterization of parts fabricated using fused deposition modeling, Rapid Prototyping Journal 9 (4) (2003) 252–264. doi:Doi10.1108/13552540310489631.
URL <GotoISI>://WOS:000184911900008

[31] H. Wadley, Cellular Metals Manufacturing, Advanced Engineering Materials 4 (10) (2002) 726–733. doi:10.1002/1527-2648(20021014)4:10<726::AID-ADEM726>3.0.CO;2-Y.
URL http://doi.wiley.com/10.1002/1527-2648(20021014)4:10<726::AID-ADEM726>3.0.CO;2-Y

[32] 3D Systems Corporation, Accura 55 plastic broucher (2007).
URL http://crdm.co.uk/pdf/Accura{_}55{_}plastic{_}MDS.pdf

[33] Z. Liu, X. Zhang, Y. Mao, Y. Zhu, Z. Yang, C. Chan, S. Ping, Locally Resonant Sonic Materials, Science 289 (2000) 1734–1736. doi:10.1126/science.289.5485.1734.
URL http://www.sciencemag.org/cgi/doi/10.1126/science.289.5485.1734

[34] P. Sheng, X. Zhang, Z. Liu, C. Chan, Locally resonant sonic materials, Physica B: Condensed Matter 338 (1-4) (2003) 201–205. doi:10.1016/S0921-4526(03)00487-3.
URL http://linkinghub.elsevier.com/retrieve/pii/S0921452603004873

[35] B. K. Lee, K. J. Kang, A parametric study on compressive characteristics of Wire-woven bulk Kagome truss cores, Composite Structures 92 (2010) 445–453. doi:10.1016/j.compstruct.2009.08.029.

[36] Y.-F. Wang, Y.-S. Wang, Multiple wide complete bandgaps of two-dimensional phononic crystal slabs with cross-like holes, Journal of Sound and Vibration 332 (8) (2013) 2019–2037. doi:10.1016/j.jsv.2012.11.031.
URL http://linkinghub.elsevier.com/retrieve/pii/S0022460X1200925X

[37] C. C. Claeys, K. Vergote, P. Sas, W. Desmet, On the potential of tuned resonators to obtain low-frequency vibrational stop bands in periodic panels, Journal of Sound and Vibration 332 (6) (2013) 1418–1436. doi:10.1016/j.jsv.2012.09.047.
URL http://linkinghub.elsevier.com/retrieve/pii/S0022460X1200853X

[38] Y. Xiao, J. Wen, G. Wang, X. Wen, Theoretical and Experimental Study of Locally Resonant and Bragg Band Gaps in Flexural Beams Carrying Periodic Arrays of Beam-Like Resonators, Journal of Vibration and Acoustics 135 (4) (2013) 041006. doi:10.1115/1.4024214.
URL http://vibrationacoustics.asmedigitalcollection.asme.org/article.aspx?doi=10.1115/1.4024214

[39] M. Petyt, Introduction to Finite Element Vibration Analysis, Cambridge University Press, 1998.
URL http://books.google.co.uk/books?id=QUTHYCAtRhcC

[40] L. Brillouin, Wave Propagation In Periodic Structures, McGraw-Hill Book Company, 1946.